29 May 1991

Beam Dynamics in RF-Gun Semi-Analytical Approach

(longitudinal motion)

Tsumoru SHINTAKE

on leave from KEK, Oho 1-1, Tsukuba, Ibaraki 305 Japan

Abstract

The beam dynamics in the radio-frequency electron gun has been studied by semi-analytical method, that is, the one-dimensional equation of motion for one electron in the pure-sine standing-wave has been solved by numerical integration. The mirror-charge on the cathode, and space-charge effects are taken into account analytically in this equation.

The calculations are applied to the CTF rf-gun, and the results are compared with the simulation results[1] of TBCI-SF.

1. Introduction

For the calculation of beam dynamics in rf-gun, we must take into account the following effects, also schematically shown in Fig. 1.1.

(1) rf-fields
    Dominant component + space harmonic component
    and field leakage effect into the beam pipe.
(2) Mirror charge effect on the cathode.
(3) Space charge effect (internal force)
(4) Wake field effect.

In the present paper, one-dimensional equation of motion in the pure standing wave is solved in numerically. The mirror charge and space charge effects are analytically estimated and taken into account in this equation. In the real rf-gun, the rf-field in the second cavity leakes into the beam pipe, which enlarges the effective wavelength in the cavity. This effect is also examined. At present paper, the wake field effect is not yet considered. However, this effect can also be taken into account in our semi-analytical calculation easily.

2. Pure sinsoidal rf-field (no space-harmonics, no leakage field)

We suppose the rf-field in the rf-gun as

$$E_z = E_c \cdot \sin(\omega t + \phi_0) \cdot \cos(kz) \qquad (2.1)$$

This is a pure sinsoidal field, not any distortion, and no leakage field in the beam pipe. From Maxwell equation of div**E**=0, we have

$$\begin{aligned} E_r &= -\frac{1}{2} r \frac{\partial E_z}{\partial z} \\ &= -\frac{1}{2} rkE_c \cdot \sin(\omega t + \phi_0) \cdot \cos(kz + \frac{\pi}{2}) \end{aligned} \qquad (2.2)$$

From $\mathrm{rot}\mathbf{H} = \varepsilon_0 \cdot \frac{\partial \mathbf{E}}{\partial t}$, we have

$$H_\theta = \frac{1}{2} r\omega\varepsilon_0 \cdot E_c \cdot \sin(\omega t + \phi_0 + \frac{\pi}{2}) \cdot \cos(kz) \qquad (2.3)$$

The approximated field patterns are schematically shown in Fig. 2.1. Here, it must be noticed that, the wavelength of E_z is just equal to the free-space wavelengh of microwave. Such field does not have radial dependence on E_z, and the transverse fields E_r and H_θ become linear fields, and provide linear focusing.

Sometimes it is usefull to represent the standing wave in the form of the travelling waves, because the standing wave is consisted from superposition of two travelling waves, each of which propagates in the opposit longitudinal directions.

$$E_z = E_a \ \{ \sin \phi_f + \sin \phi_b \} \qquad (2.4a)$$

$$E_r = \frac{1}{2} rkE_a \ \{ \cos\phi_f - \cos\phi_b \} \qquad (2.4b)$$

$$H_\theta = \frac{1}{2} r\omega\varepsilon_0 \cdot E_a \ \{ \cos\phi_f + \cos\phi_b \} \qquad (2.4c)$$

where E_a is average accelerating gradient at peak phase on the pure travelling-wave, which is just equal to half of the cathode field.

$$E_a = \frac{1}{2} E_c \qquad (2.5)$$

ϕ_f and ϕ_b are the phase of the forward and the backward wave components.

$$\phi_f = \omega t - kz + \phi_0 \qquad (2.6a)$$

$$\phi_b = \omega t + kz + \phi_0 \qquad (2.6b)$$

3. Longitudinal Beam Motion in the rf-field

Electrons emitted from the photocathode are quickly accelerated by high gradient rf-field. However the electron energy near the cathode is not relativistic, it experiences large phase slip. In order to estimate this effect, it is possible to approximate the rf-field by the static field near the cathode as ref. (2). However, this analytical method has large error for small initial phase. In this report, instead of such approximation, we numerically integrate the following equation of motion.

$$\frac{d\gamma}{dz} = \frac{qE_c}{m_0c^2}\cdot\sin(\omega t + \phi_0)\cdot\cos(kz)$$

$$= 2k\alpha\cdot\sin(\ \phi + kz\ )\cdot\cos(kz) \qquad (3.1)$$

where α is normalized accelerating gradient, same definition as ref. (2).

$$\alpha = \frac{qE_a}{m_0c^2k} = \frac{qE_c}{2m_0c^2k} \qquad (3.2)$$

Nominal parameter of CTF rf-gun are; E_c = 100 MV/m at S-band (3 GHz), α = 1.56. ϕ is the particle phase (beam phase) as refered to the travelling wave component,

$$\phi = \omega t - kz + \phi_0 \ (= \phi_f\ )$$

$$= k\int_0^z (\frac{\gamma}{\sqrt{\gamma^2 - 1}} - 1)\cdot dz + \phi_0 \qquad (3.3)$$

By integrating eqs(3.1) and (3.2), we can get the beam trajectory as shown in Fig. 3.1. Each line shows trajectory of different electron which has been started from the cathode at different phases of 10 degrees intervals. Near the cathode, the electron energy is non relativistic, so that the trajectories are curved. However after only 1 cm passage, they becomes straight lines because the velocity reaches the velocity of light.

The electrons which started at ϕ_0 between140 to 180 degrees can not ride on the wave and returen to the cathode. This is the back-bombarding effect. Of course, from 180 to 360 degree, the cathode field is negative and no any electron can go out from the cathode. If we observe the electron trajectory on the travelling wave, we can see the electron phase more clearly as shown in Fig. 3.2. The end wall of the second cavity is $kz = 1.5\pi$. The electron shows large phase slip near the cathode, so that the final phase (at $kz = 1.5\pi$) is always greater than the initial phase (laser ilumination phase). For example, for initial phase of 30 deg, the final phase is 53 deg.

By plotting the final phase as a function of the inital phase, we can get the phase diagram as shown in Fig. 3.3. The phase slip plays very important role on the beam behavior in rf-gun, so that this phase diagram is very important to explain the beam dynamics in the rf-gun.

3.1 Bunch Length

From the phase diagram, we can easily estimate the bunch length for small charge case. Letting the laser beam length as Δt (FWHM), and corresponding phase width $\Delta\phi_0$. In the form of root mean square,

$$\sigma_t^{\,2} = <\delta t^{\,2}> = \int_{-\Delta t/2}^{\Delta t/2} \delta t^{\,2} \cdot \delta t \; = \frac{\Delta t^2}{12}$$

$$\sigma_t = \frac{\Delta t}{2\sqrt{3}} \qquad (3.4)$$

In the CTF case,

Δt	30	psec
$\Delta\phi_0$	32.4	degree
$\sigma_{\phi 0} = \frac{\Delta\phi_0}{2\sqrt{3}}$	9.4	degree

The bunch length at the exit of the cavity is given by

$$\Delta\phi = \frac{d\phi}{d\phi_0}\cdot\Delta\phi_0 \qquad (3.5)$$

$d\phi/d\phi_0$ is slope of the curve of the phase-diagram, also called the bunch compression ratio, which is plotted in Fig. 3.4. As seen in the figure, for a lower value of the initial phase, the compression ratio is less than one, which means the bunch will be compressed during the acceleration, but for larger value of initial phase the bunch length becomes longer than the initial value. For CTF rf-gun case, the expected bunch length is shown in Fig. 3.5. The circular marks are results by the particle-in-cell simulation[1] using TBCI-SF for the following nominal parameters,

Table-3.1 Nominal CTF rf-gun parameters.

Cathode Field	E_c	100 MV/m
Pulse Length	Δt	30 psec
Cathode Radius	r_c	5 mm
Charge per pulse	Q	9.4 nC

It must be noted that in ref. (1), "the laser phase" is defined as the rf-phase at the begining of the laser beam, but in the present paper we define the initial phase as the center of the laser pulse. Hence, we must shift the initial phase −16.2 deg. in the ref. (1).

As seen in the figure, our simple model can provide almost correct values for the bunch length. However, at the smaller initial phase, the rf-fields tends to compress the bunch to very small size, but due to the space charge repulsion force, the bunch can not be compressed to such smaller size. In our simple model the space charge force is not included, so that the curve takes zero beam size at initial phase of 5 degree.

3.2 Energy Gain

The electron energy does not go up smoothly but sinously as shown in Fig. 3.6. The longitudinal force acting on an electron is, from eq.(2.4a),

$$F_z = qE_z$$

$$= qE_a \{ \sin\phi + \sin(2kz+\phi) \} \qquad (3.6)$$

If the electron is relativistic, the electron phase does not change, so that the first term is constant, which represents the constant energy gain on the travelling wave component. The second term represents the energy modulation effect due to the interaction with the backward wave component, which is half-wavelength oscillation, in case of CTF this period is 5 cm. The equation of motion is

$$\frac{dP_z}{dt} = qE_z \qquad (3.7)$$

In order to see the basic mechanism, here we approximate the electron being already relativistic, $v = c$, and ϕ is constant, then we have the approximated energy gain

$$\gamma = 1 + \alpha [kz\cdot\sin\phi - \frac{1}{2} \{ \cos(2kz+\phi) - \cos\phi \}] \qquad (3.8)$$

For the $\frac{1}{2}$ + 1 cell cavity, the final energy is given by letting $kz = 1.5\pi$,

$$\begin{aligned} \gamma &= 1 + \alpha [(1+\frac{1}{2})\pi\cdot\sin\phi + \cos\phi] \\ &= 1 + 4.81\ \alpha\cdot\sin(\phi + 12 \text{ deg}) \end{aligned} \qquad (3.9)$$

Hence, the accelerated electron takes its maximum energy at peak phase of

$$\phi_{peak} = 90 - 12 = 78 \text{ deg.} \qquad (3.10)$$

The energy gain curve is symmetric according to this peak phase on the (ϕ , γ)-plane. However, as already described, near the cathode the electron experiences the phase-slip, so that the energy gain curve has an asymmetric shape on (ϕ_0, γ)-plane. This is schematically shown in Fig. 3.7, and numerical results of our simple model are shown in Fig.3.8, where the numerical simulation results by TBCI-SF are also plotted. As seen in

the figure, our model can explain this asymmetry in qualitatively, however the quantitative agreement is poor. As seen in the later sections, this is mainly due to the field leakage effect into the beam pipe.

3.3 Energy Spread

By derivating the energy gain function, we can get the energy spread as follows.

$$\sigma_\gamma = \frac{d\gamma}{d\phi_0} \cdot \sigma_{\phi 0} \tag{3.11}$$

In Fig. 3.9, the calculated energy spread is shown. The simple model can explain the characteristic property of energy spread qualitatively, however the agreement with the TBCI-SF is not so good.

4. Mirror Charge Effect

When the electron bunch departs from the cathode, the mirror image on the cathode try to pull-back the bunch to the cathode, because the image has opositte polarity charge. This is the mirror charge effect, which cause the additional phase delay on the beam starting from the cathode.

Here we treat this problem by a simple disk-model as shown in Fig. 4.1. We replace the electron bunch by a disk of zero-thickness and radius r_c, of charge $+Q$, and which position is $+z$ from the cathode, and running with $+v$ velocity. The image charge has $-Q$ charge, running with $-v$ velocity at $-z$. If we observe the image charge on the electron rest frame the distance between two disk charge becomes longer: $\gamma \cdot 2z$, due to the relativistic effect.

However, shown in later, this mirror effect is effective only near the cathode, and in this region the electron energy is not yet relativistic, so that, we can treat this field as a non-relativistic and static field. When the disk to disk spacing is smaller than its radius, we can approximate the field as a parallel field between two plane charge as shown in Fig. 4.2. From the Gauss's theorem, we have

$$E_{z\cdot\mathrm{mir}}{}^{0} = \frac{\sigma_0}{2\varepsilon_0} = \frac{-Q}{2\pi\varepsilon_0 r_c{}^2} \tag{4.1}$$

This field is constant and is not a function of the distance.

When the spacing of two disks becomes much larger than its transverse dimensions, the field becomes point-charge field. In this case the field is

$$E_{z\cdot mir} = \frac{-Q}{4\pi\varepsilon_0 R^2} \tag{4.2}$$
$$R = 2z$$

The mirror field takes constant value of $E_{z\cdot\mathrm{mir}}{}^{0}$ when the bunch stays near the cathode, and after departing from the cathode the field decays according to R^{-2}. Here, we approximate this field as a square shaped field, which intensity is equal to the initial field and effective spacing is $R = r_c$, where the point like field takes half the value of $E_{z\cdot\mathrm{mir}}{}^{0}$. The effective distance from the cathode is

$$z_{mir} = \frac{r_c}{2} \tag{4.3}$$

In the CTF case, z_{mir} = 2.5 mm, corresponding average electron energy is about 100 MV/m x 2.5 mm = 250 keV. The mirror field for 9.4 nC charge is $E_{z\cdot\mathrm{mir}}{}^{0}$ = – 6.8 MV/m, which is about 7 % of peak cathode field.

By taking account this field into the equation of motion, we get the phase diagram, bunch length and energy gain curves as shown in Fig. 4.3 to 4.5. It is evident in the figure that the mirror effect provides the additional phase slip on the beam, which is about 10 deg for small initial phase, and a few deg. at the nominal inital phase of 50 deg.

5. Space Charge Effect

The space charge creates repulsion force between electrons, which cause energy spread and bunch lengthening in longitudinal motion, and beam spread in radial direction. This force is internal force, so that it does not make any effect on the beam energy gain in the first order

approximation. The non-linear component of space charge force cause the emittance growth. Here we consider the linear longitudinal parts only.

Because of the repulsion force, after the acceleration the bunch has energy spread, that is, electrons at the head have higher energy than that in the tail as shown in Fig. 5.1. We calculate this energy spread by two-disks model. Dividing the electron bunch in two volumes, head and tail, and replacing these charges by two disk charges. If the full length of bunch is Δz, the disk spacing is $\Delta z/2$. In the electron rest frame, the spacing is larger that that in laboratory frame,

$$s' = \gamma s = \gamma \frac{\Delta z}{2} \tag{5.1}$$

The repulsion force takes just same variation as mirror charge force, but its sign is positive (repulsion force). The force takes constant value when the disk spacing is small, and dcreases according to its spacing increase as shown in Fig. 5.2. Increasing the beam energy, γ becomes large, the disk spacing in electron rest frame becomes large, and the repulsion force decreases. During this process, the head electrons accept some amount of kinetic energy from the tail electrons. We can calculate this energy gain as follows.

$$\frac{\Delta \gamma_{sp}}{4} = \frac{1}{m_0 c^2} \int_0^{\infty} q E_{z.sp}(s') \cdot dz \tag{5.2}$$

To perform this integration, we need to know the variation of the bunch length. For simplification, here we approximate the bunch length as a constant

$$\Delta z = c \cdot \Delta t \tag{5.3}$$

where Δt is the laser pulse length. Additionally, we approximate the constant energy gain, that is,

$$\gamma = 1 + 2\alpha \cdot \sin\phi_0 \cdot kz \tag{5.4}$$

Then,

$$\frac{ds'}{dz} = \frac{\Delta z}{2}\cdot\frac{d\gamma}{dz} = \alpha\cdot k\Delta z\cdot\sin\phi_0 \qquad (5.5)$$

The integration becomes

$$\begin{aligned}\frac{\Delta\gamma_{sp}}{4} &= \frac{1}{m_0c^2}\int_{s_0'}^{\infty} qE_{z.sp}(s')\cdot\frac{dz}{ds'}\cdot ds' \\ &= \frac{1}{m_0c^2}\int_{s_0'}^{\infty} qE_{z.sp}(s')\cdot\frac{1}{\alpha\cdot k\Delta z\cdot\sin\phi_0}\cdot ds' \\ &= \frac{q}{m_0c^2}\cdot\frac{\Phi_{sp}}{\alpha\cdot k\Delta z\cdot\sin\phi_0} \qquad (5.6)\end{aligned}$$

where Φ_{sp} is a kind of potential energy which is stored in the initial bunch when the bunch is emerged from the cathode. This potential energy is transfered to the kinetic energy during the acceleration.

Here, we call Φ_{sp} as "longitudinal space-charge potential".

To estimate Φ_{sp}, we must know the initial disk spacing s_0', which depends on the laser pulse length and accelerating gradient. In order to simplify, we let $s_0' = 0$.

$$\Phi_{sp} = \int_0^{\infty} E_{z.sp}(s')\cdot ds' = \int_0^{rc/\sqrt{2}} E_{z.sp}{}^0\cdot ds' + \int_{rc/\sqrt{2}}^{\infty}\frac{Q}{8\pi\varepsilon_0 s'^2}\cdot ds' \qquad (5.7)$$

$$\Phi_{sp} = \frac{\sqrt{2}Q}{4\pi\varepsilon_0 r_c} \qquad (5.8)$$

Finally we have the energy spread due to the space charge effect as follows.

$$\Delta\gamma_{sp} = 4 \cdot \frac{q\Phi_{sp}}{m_0 c^2} \cdot \frac{1}{\alpha \cdot k\Delta z \cdot \sin\phi_0} \tag{5.9a}$$

$$\sigma_{\gamma sp} = \frac{\Delta\gamma_{sp}}{2\sqrt{3}} \tag{5.9b}$$

$$\frac{\sigma_{\gamma sp}}{<\gamma>} \approx \frac{2}{\sqrt{3}} \cdot \frac{\Phi_{sp}}{E} \cdot \frac{1}{\alpha \cdot k\Delta z \cdot \sin\phi_0} \tag{5.9c}$$

where E is the beam energy in eV.

Here we must point out the important fact that if the bunch stays in the lower phase side than the peak energy phase as shown in Fig. 5.3, the energy spreads due to rf-effect and the space-charge effect canceles each others, on the other hand, at the higher phase position, these energy spreads are summed up and cause larger energy spread.

In the CTF-case,

Q = 9.4 nC, r_c = 5 mm
Φ_{sp} = 23.9 kV
$\sigma_{\gamma sp}$ = 36.2 keV (at ϕ_0 = 90 deg)
72.4 keV (at ϕ_0 = 30 deg)
$\frac{\sigma_{\gamma sp}}{<\gamma>}$ = 1.0 % (at ϕ_0 = 90 deg)
2.0 % (at ϕ_0 = 30 deg)

Figure 5.4 shows energy gain and energy spread, as compared with TBCI-SF for 9.4 nC charge and zero charge cases (1pC). From the differences between two cases of TBCI-SF we can approximately estimate the energy spread due to space charge effect (it must be noticed that the space charge and mirror charge effects are always mixed in the simulation, and we can not separate perfectly). The simulated energy spread due to space charge effect is 0.8 % around 20 deg. initial phase, and 1.2 % at 80 deg. initial phase. Hence, our analytical expression can provide almost correct value of energy spread at large initial phase, but at the small initial phase the simulation shows smaller energy spread than the analytical one. This may be due to the bunch compression effect by the rf-field, but it is not yet clear.

6. Effect of rf-field leakage into beam pipe.

In the previous sections, we have calculated the beam dynamics in the pure-sine standing-wave fields, and examine the mirror charge and space charge effects on the energy gain, bunch length and the energy spread. However, the agreements of these calulated results were not so good. This is mainly due to the rf-field leakage effect into the beam pipe as seen below.

Indeed the practical rf-field in the rf-gun has higher order space harmonic components, but its effect is small because the rf-cavity has been designed to have good field patterns[3] (pure-sine wave or small distortions). Fig. 6.1 shows the real rf-field in the rf-gun simulated by TBCI-SF. The dotted curve shows the aproximated sine-wave of 10 cm wavelength. As seen in the figure clearly, in the first cell the real field pattern quite agrees with the pure-sine wave, but in the second cell, due to the field leakage into the beam pipe the effective cavity length becomes larger than the ideal length. We can approximate this effect by introducing the effective wavelength, which is 12.8 cm in the second cavity as shown in Fig. 6.2(a). In the orther words, the phase velocity in the second cell is 12% higher than the velocity of the light. At the beam edge, r = 5 mm, the field pattern is not so different from the axial values as shown in Fig. 6.2(b).

By taking into account this field leakage effect, the beam energy and energy spread are calculated as shown in Fig. 6.3. The agreement with the numerical simulation becomes much better than with the simple sine-wave case. The error in energy spread at the lower initial phase due to the fact that in the analytical estimation we have taken the bunch length as a constant, but in the real rf-gun the bunch length becomes smaller at the lower initial phase which makes the energy spread lower.

7. Summary

The beam dynamics in rf-gun has been studied by solving the one-dimensional equation of motion in numerically, by taking into account the mirror charge effect and space charge effect analytically. The calculated results well agreed with the numerical simulation results of TBCI-SF.

Through this study, it has been found that, in the CTF rf-gun, due to the rf-field leakage into the beam pipe, the effective wavelength in the second cell is 12% greater than the ideal wavelength, which has substantial effect on the beam properties.

In the present paper, we have calculated the longitudinal motion only. Further works on the radial motion and the emittance estimation based on the same method are required for better understanding of the beam dynamics, and also for development of advanced rf-gun for CLIC project, which is required to generate very short (1 mm) high-intensity (10^{12} e^-) electron bunches.

Acknowledgement

The author wishes to thank A.J.Riche and J. Stroede for their usefull discussions on the beam dynamics in rf-gun.

References

1. J. Stroede, "Calatlogue of simulation of the CTF rf gun", PS/LP Note 90-35.

2. Kwang-Je Kim, "RF and space-charge effects in laser-driven rf electron guns", Nucl. Instrum. and Methods A275 (1989) 201-218

3. K. T. McDonald, "Design of the Laser-Driven RF Electron Gun for the BNL Accelerator Test Facility", Princeton University March 23, 1988, DOE/ER/3072-43

Figure Captions

Fig. 1.1 Four different effects in rf-gun.

Fig. 2.1 Pure-sine standing-wave approximation.

Fig. 3.1 Beam trajectory. Time in rf-phase versus beam position z.
One dimensional solution without space-charge effect.
$\alpha = 1.0$, $f = 2856$ MHz.

Fig. 3.2 Beam phase variation during the acceleration.

Fig. 3.3 The phase-diagram: Final phase as a function of initial phase for various accelerating gradient.

Fig. 3.4 Bunch compression ratio for various accelerating gradient.

Fig. 3.5 Calculated bunch size.
The analytical calculation does not include the space-charge force.

Fig. 3.6 Beam energy as a function of beam position.

Fig. 3.7 Cause of the asymmetric shape in the energy gain and energy spread curves.

Fig. 3.8 Energy gain as a function of the initial phase.
Analytical value: without mirror charge, without space-charge.

Fig. 3.9 Energy spread as a function of the initial phase.
Analytical value: without mirror charge, without space-charge.

Fig. 4.1 The mirror-charge effect. Disk-model approximation.

Fig. 4.2 Approximated mirror charge field.

Fig. 4.3 Phase diagram including the mirror charge effect.

Fig. 4.4 Bunch length including the mirror charge effect.

Fig. 4.5 Energy gain including the mirror charge effect.

Fig. 5.1 Energy spread due to space charge force.
Disk-model approximation.

Fig. 5.2 Approximated longitudinal space-charge force.

Fig. 5.3 Cancellation of the rf-induced energy spread and space-charge induced energy spread.

Fig. 5.4 Energy gain and energy spread including the space charge effect.
+ mark shows the simulation results for zero charge case.

Fig. 6.1 Axial electric field pattern simulated by TBCI-SF, and pure sin-wave of 10 cm wavelength.

Fig. 6.2 Modified sin-wave field with wavelength correction.
(a) on the axis. (b) at the beam edge (r = 5 mm)

Fig. 6.3 Energy gain and energy spread with leakage field correction.

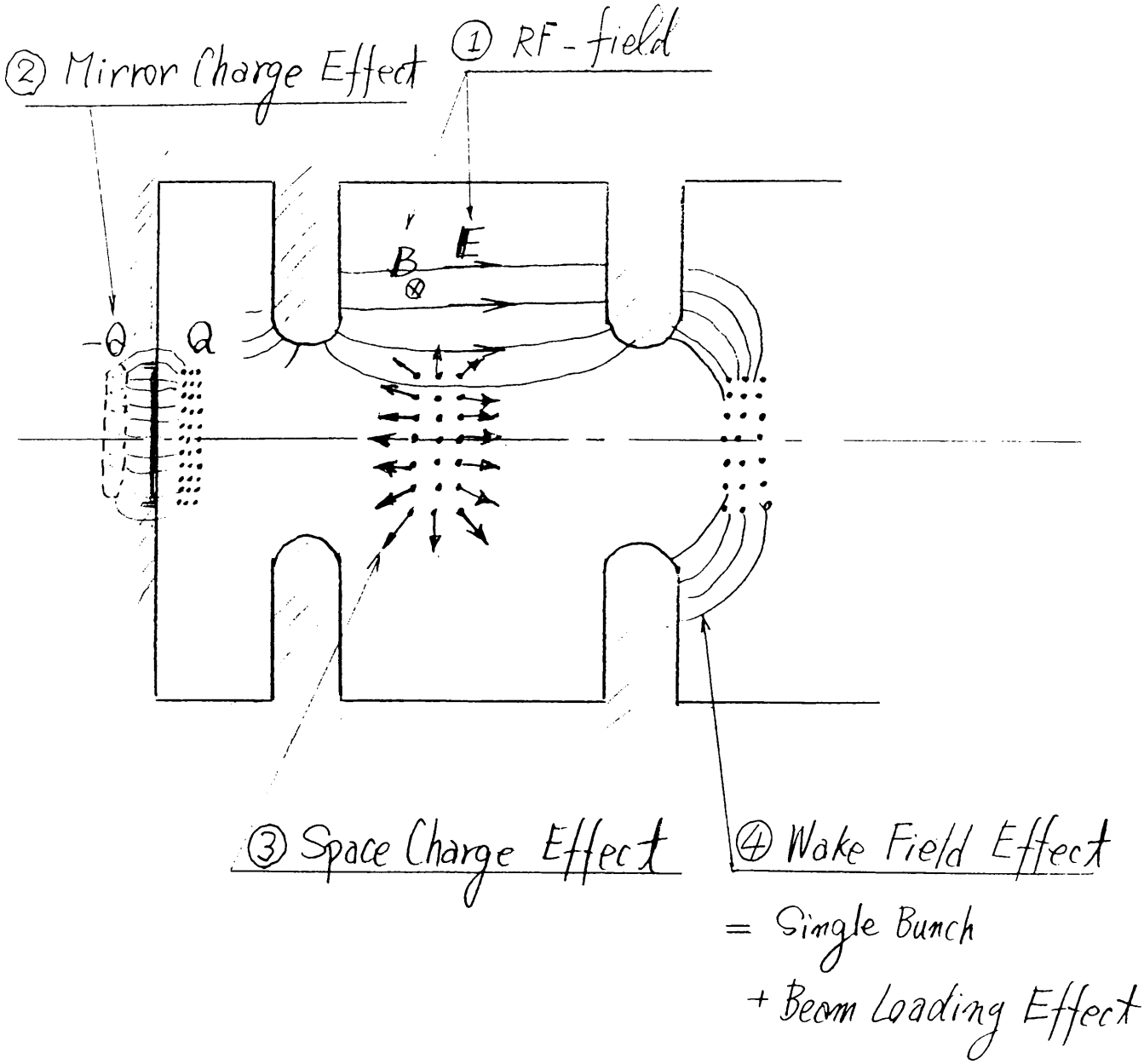
② Mirror Charge Effect
① RF - field
B
E
-Q
Q
③ Space Charge Effect
④ Wake Field Effect
= Single Bunch
+ Beam Loading Effect

Fig 1.1

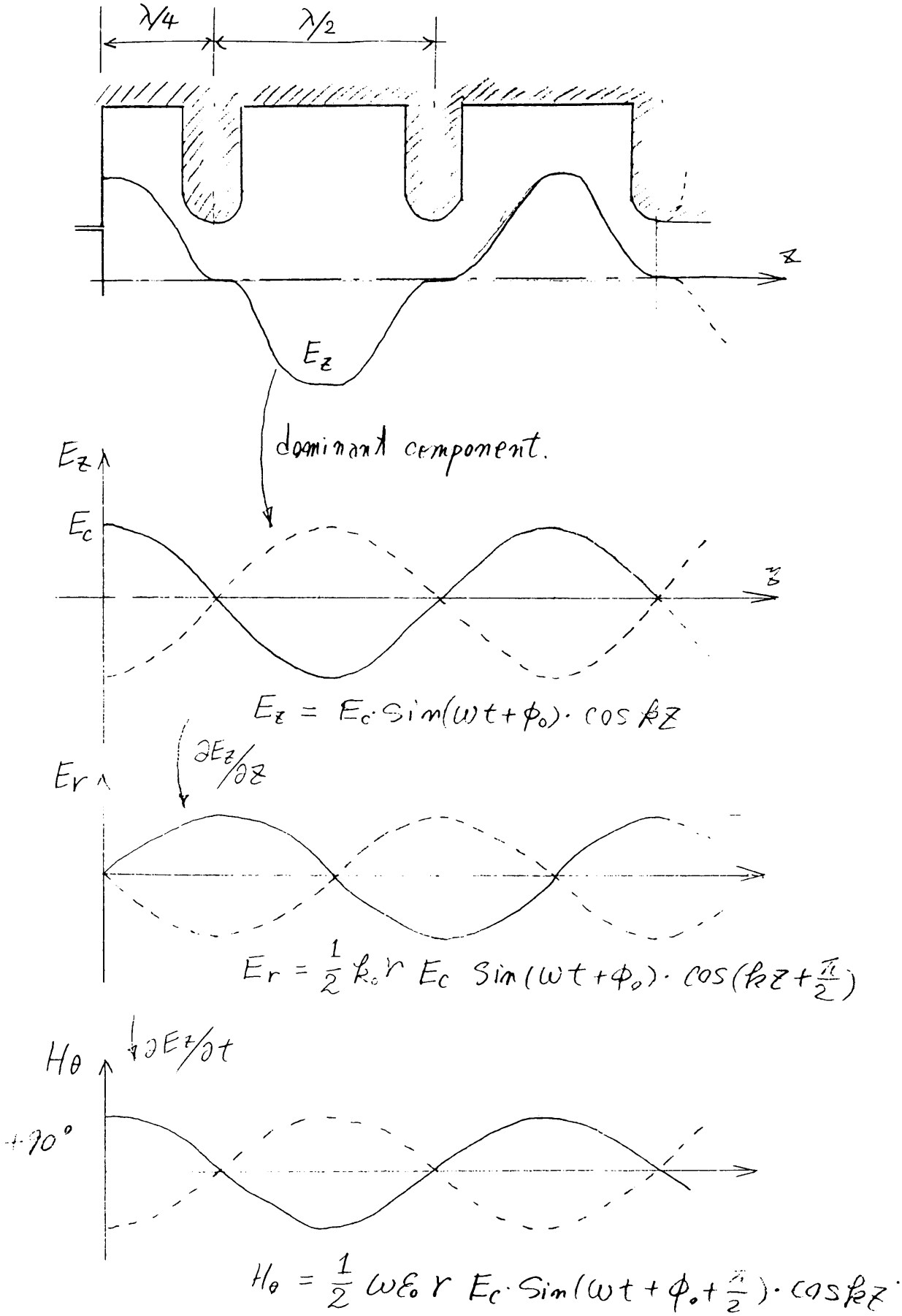
λ/4
λ/2
z
E_z
dominant component.
E_z
E_c
z
$E_z = E_c \cdot \sin(\omega t + \phi_0) \cdot \cos kz$
$\partial E_z/\partial z$
E_r
$E_r = \frac{1}{2} k_0 r E_c \sin(\omega t + \phi_0) \cdot \cos(kz + \frac{\pi}{2})$
$\partial E_z/\partial t$
H_θ
+90°
$H_\theta = \frac{1}{2} \omega \varepsilon_0 r E_c \cdot \sin(\omega t + \phi_0 + \frac{\pi}{2}) \cdot \cos kz$

Fig. 2.1

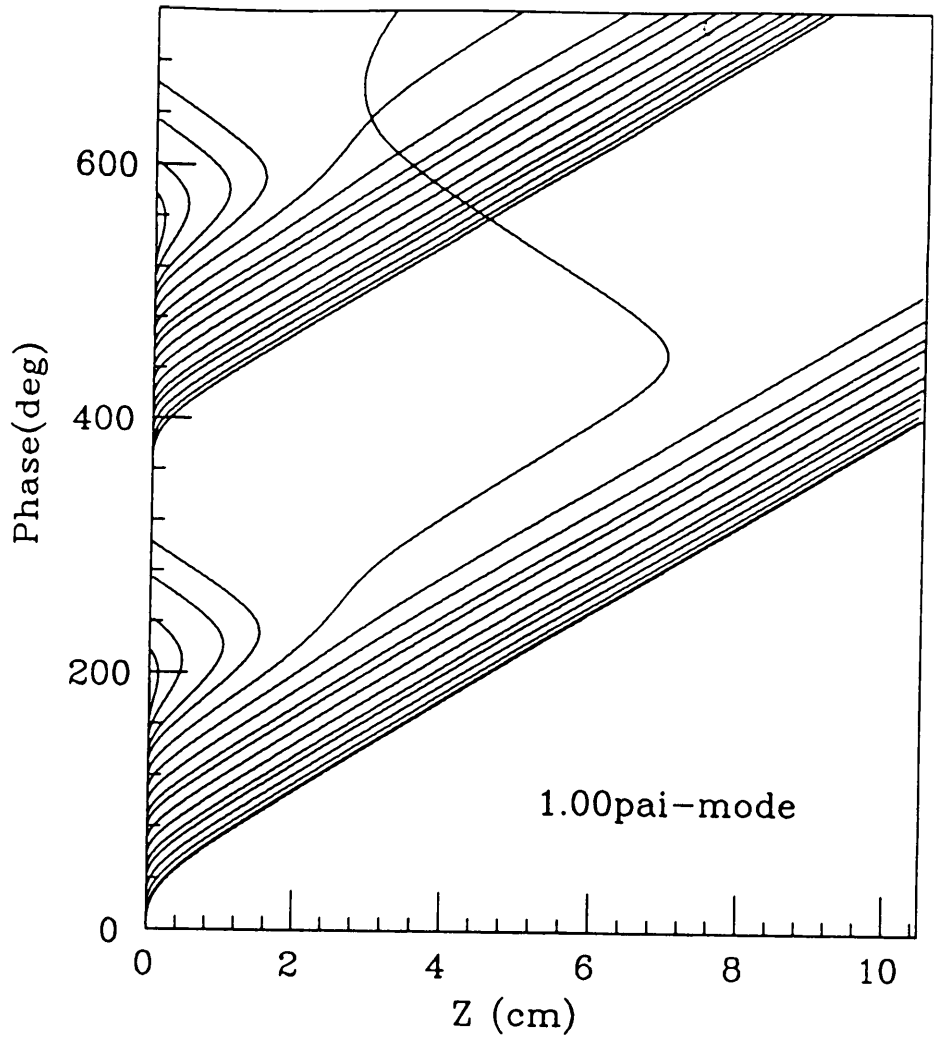
Phase(deg)
600
400
200
0
0
2
4
6
8
10
Z (cm)
1.00pai-mode

Fig. 3.1

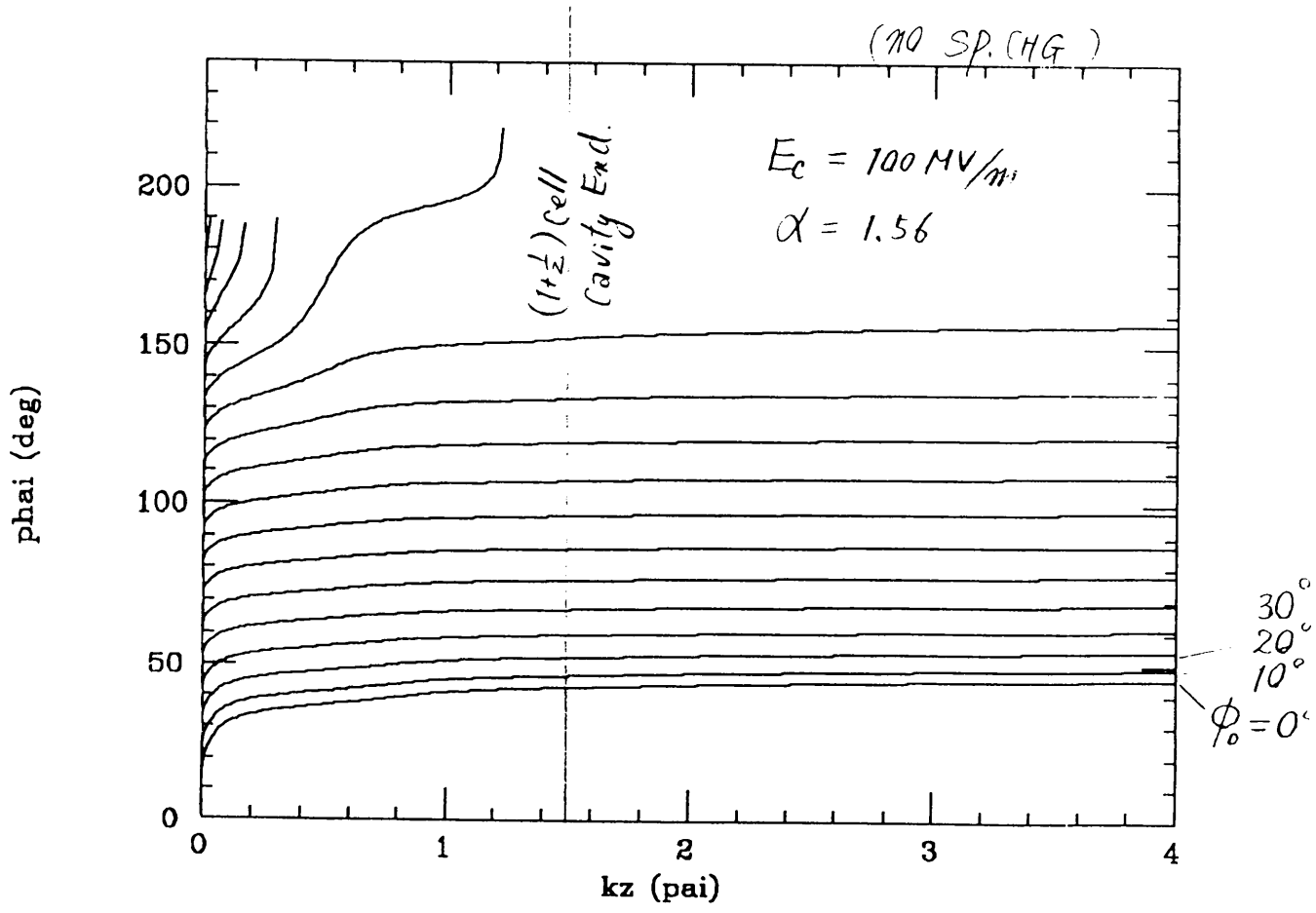
(π0 SP. CHG)
E_c = 100 MV/m
α = 1.56
(1+½) Cell
Cavity End
phai (deg)
200
150
100
50
0
0
1
2
3
4
kz (pai)
30°
20°
10°
ϕ_0 = 0°

Fig. 3.2

$\phi(\phi_0)$ - curve

$(\frac{1}{2}+1)$ cell, π-mode

(no SP. CHG.)

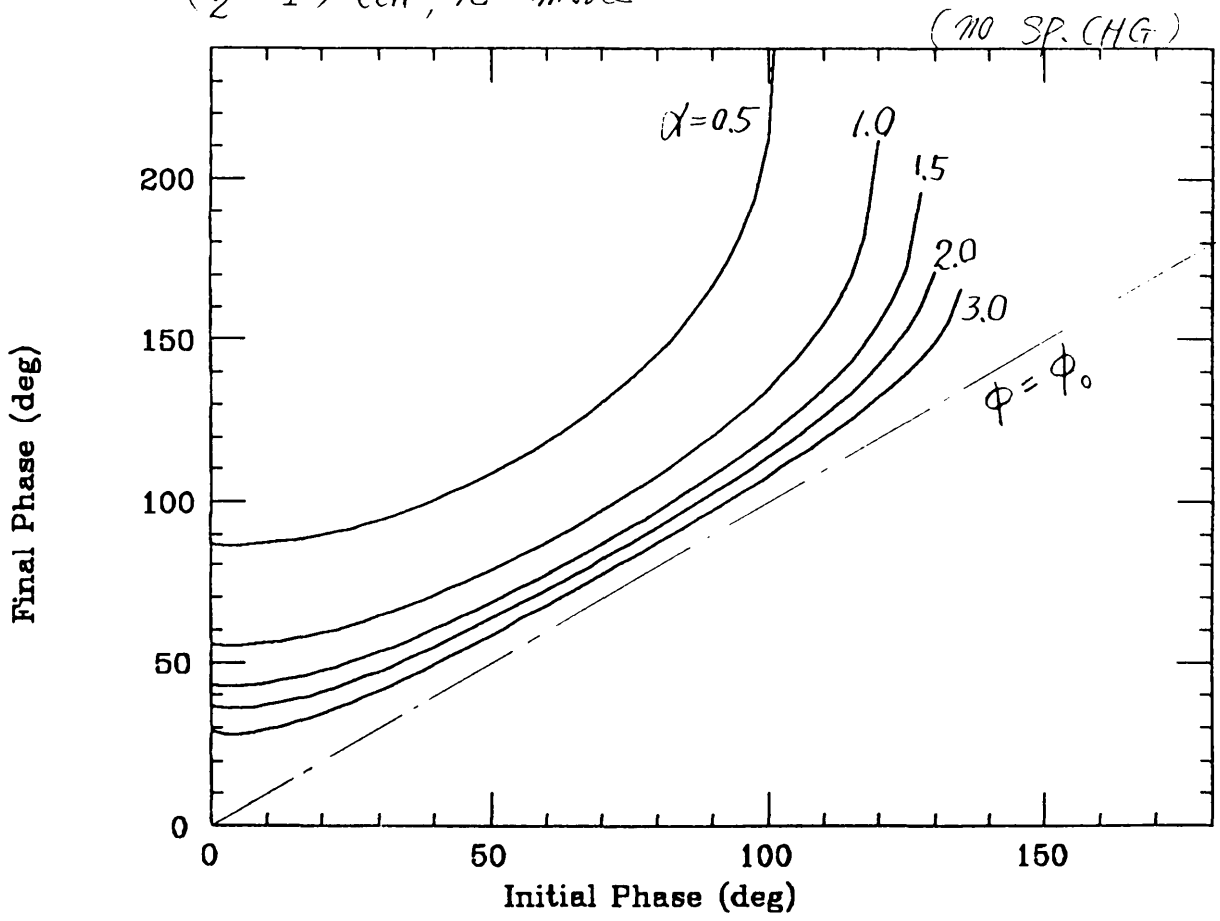

Fig. 3.3

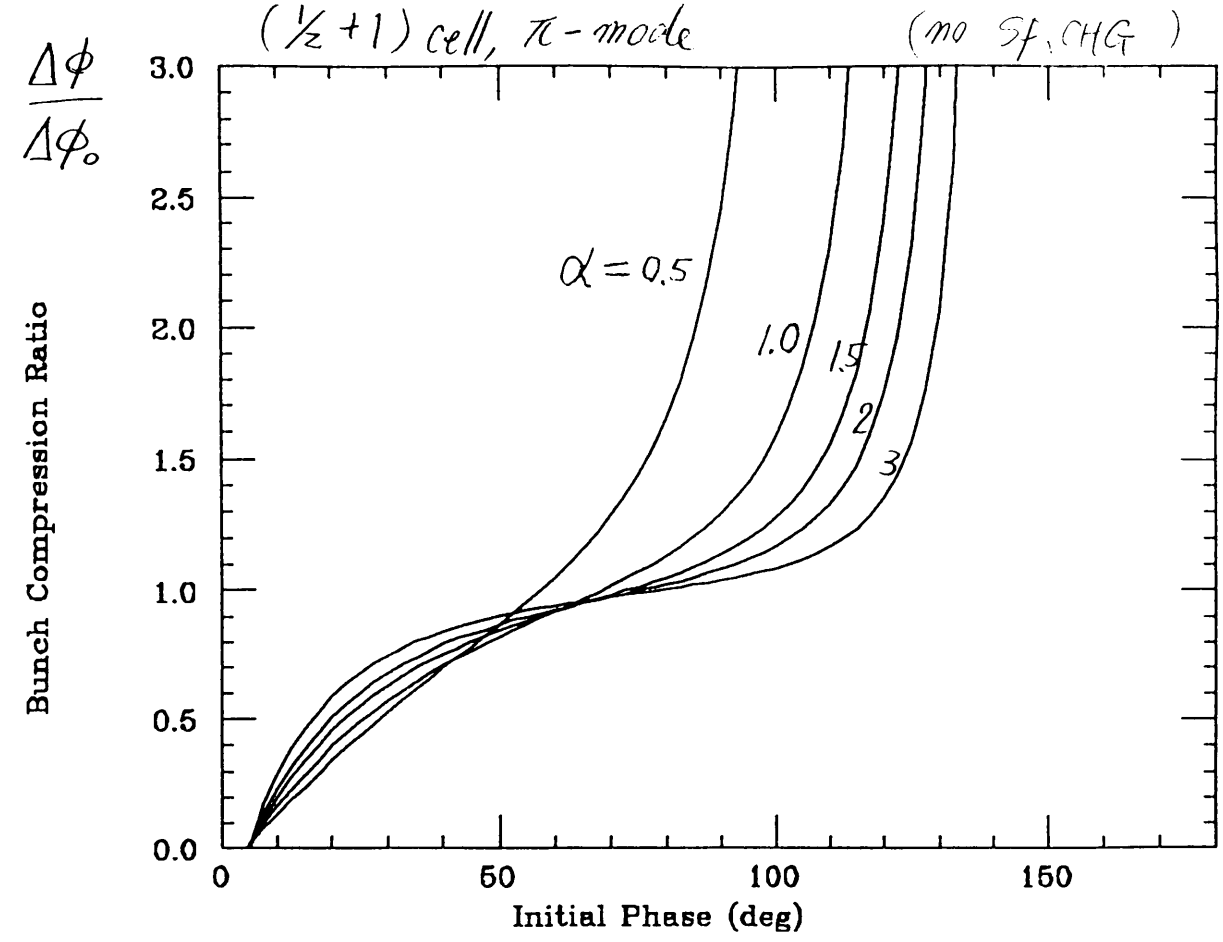
(½+1) cell, π-mode
(no Sp. CHG)
Δφ/Δφ₀
Bunch Compression Ratio
α = 0.5
1.0
1.5
2
3
Initial Phase (deg)

Fig. 3.4

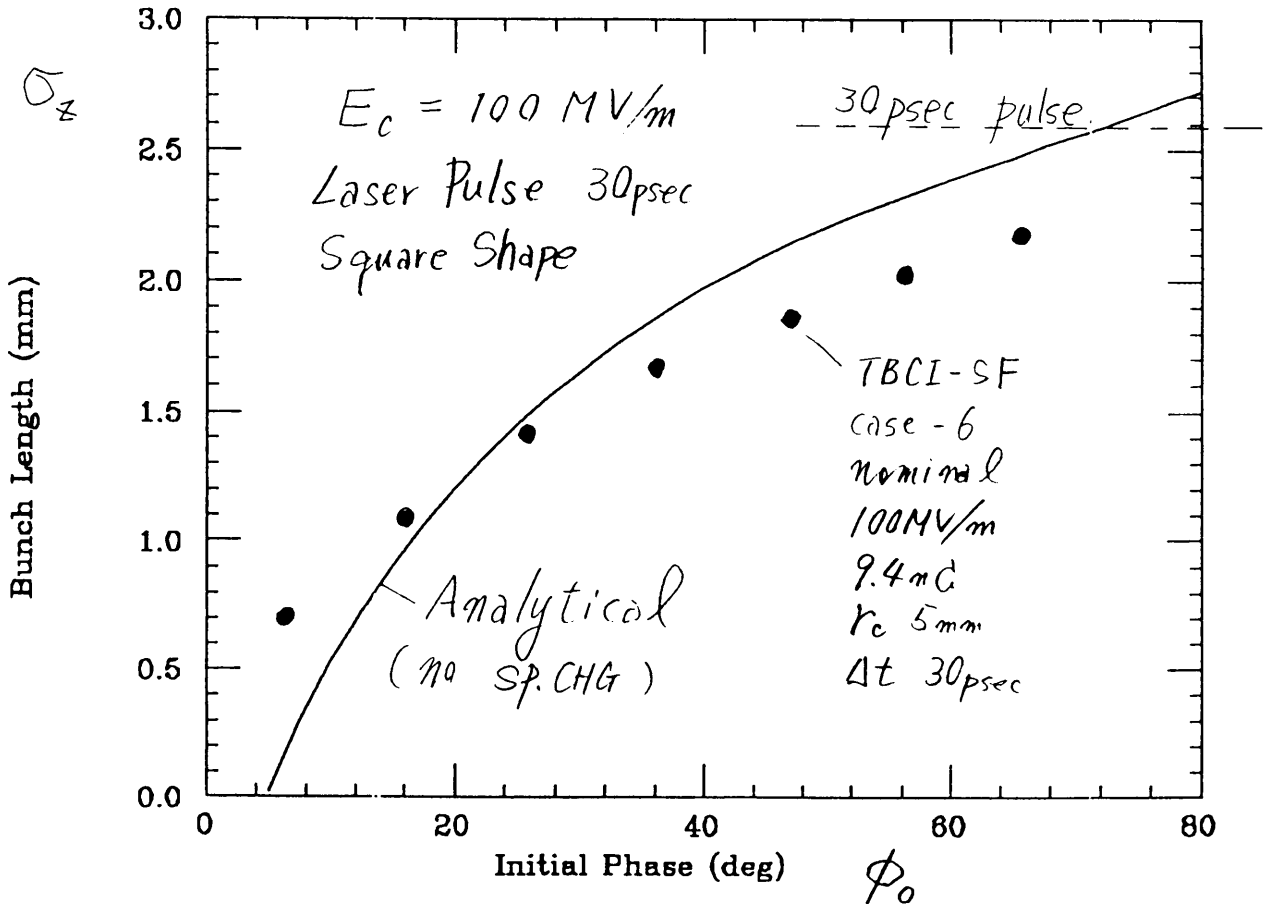
σz
Ec = 100 MV/m
30psec pulse
Laser Pulse 30psec
Square Shape
TBCI-SF
case-6
nominal
100MV/m
9.4nC
rc 5mm
Δt 30psec
Analytical
(no Sp. CHG)
Bunch Length (mm)
Initial Phase (deg)
φ₀

Fig. 3.5

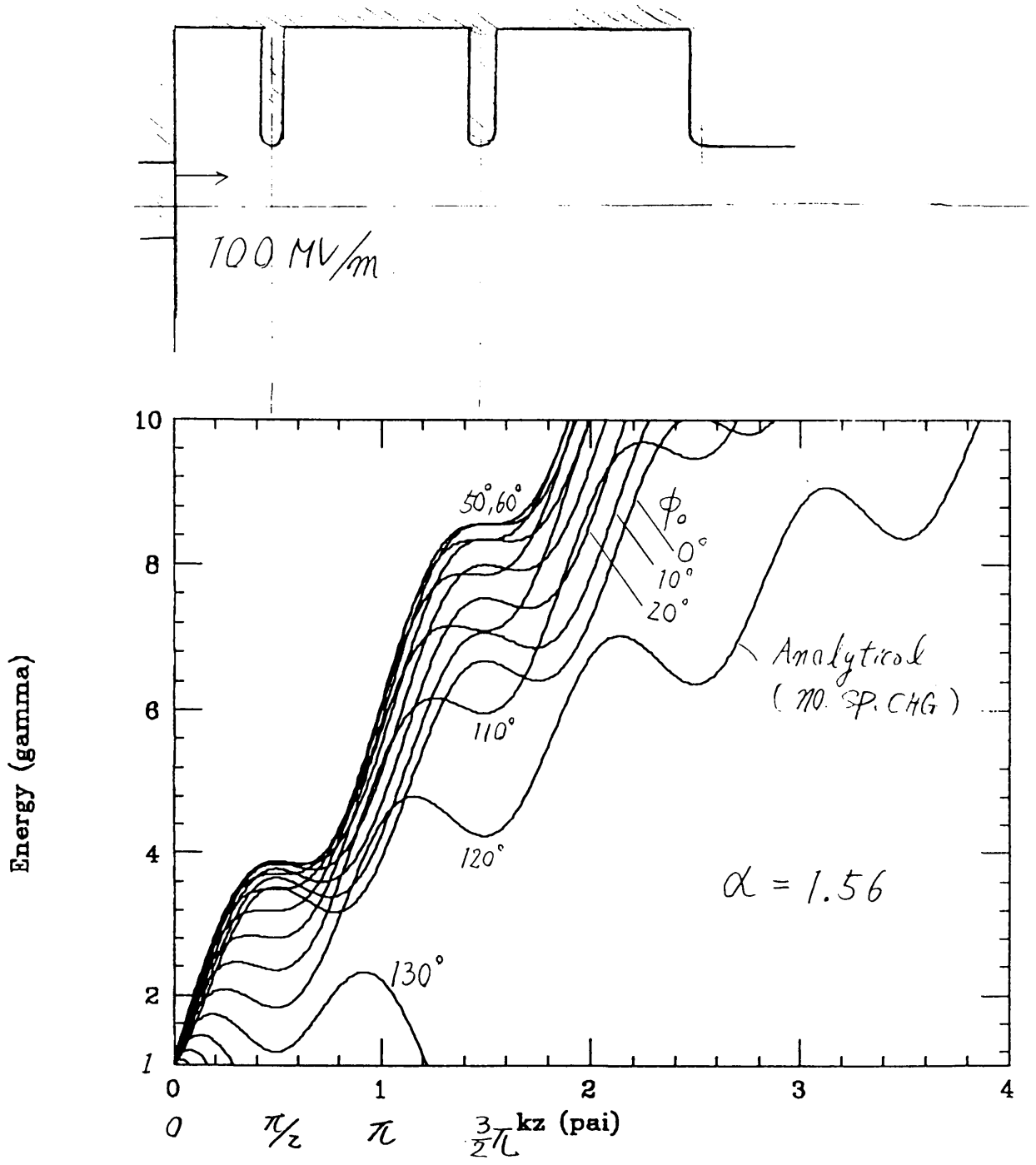
100 MV/m
Energy (gamma)
10
8
6
4
2
1
0
1
2
3
4
0
π/2
π
3/2π
kz (pai)
50°,60°
φ₀
0°
10°
20°
110°
120°
130°
Analytical
(NO SP. CHG)
α = 1.56

Fig. 3.6

Energy Gain diagram $\gamma(\phi_0)$

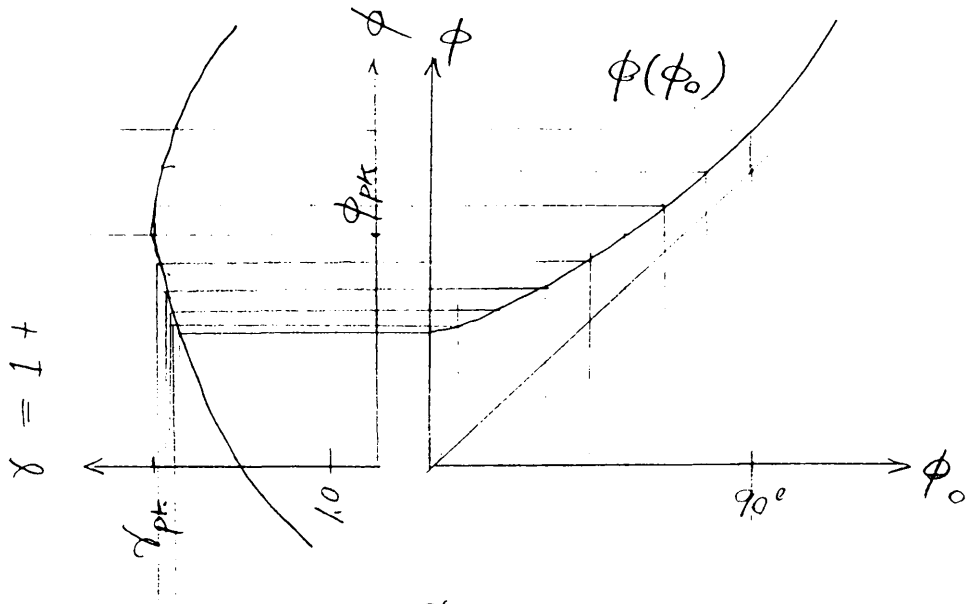

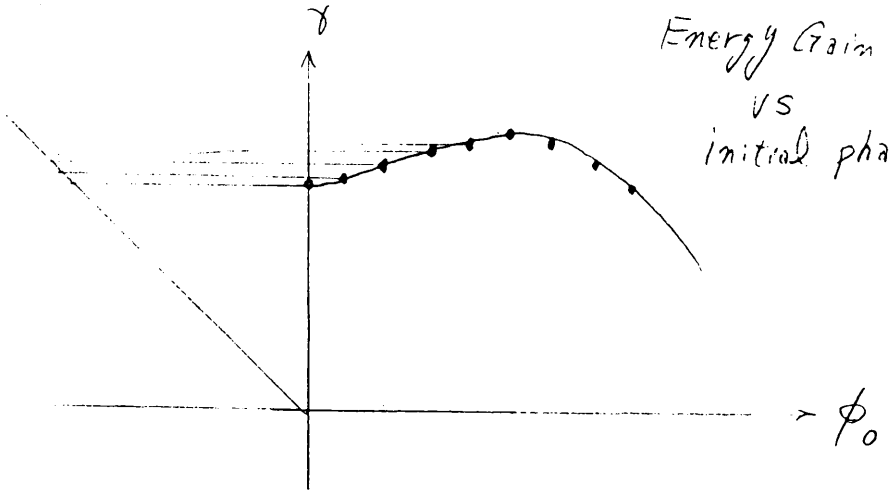

Energy Gain vs initial pha

$$\sigma_\gamma^2 = \frac{1}{\Delta\phi_0}\int_{-\Delta\phi_0/2}^{\Delta\phi_0/2} (\gamma - \langle\gamma\rangle)^2 d\phi_0$$

$$= \frac{1}{\Delta\phi_0}\left(\frac{d\gamma}{d\phi_0}\right)^2 \int \phi_0^2 d\phi_0$$

$$= \frac{1}{3}\left(\frac{d\gamma}{d\phi_0}\right)^2 \left(\frac{\Delta\phi_0}{2}\right)^2$$

$$\therefore \sigma_\gamma = \frac{1}{\sqrt{3}}\left(\frac{d\gamma}{d\phi_0}\right)\left(\frac{\Delta\phi_0}{2}\right)$$

$$= \left(\frac{d\gamma}{d\phi_0}\right)\sigma_{\phi_0},$$

9.4°

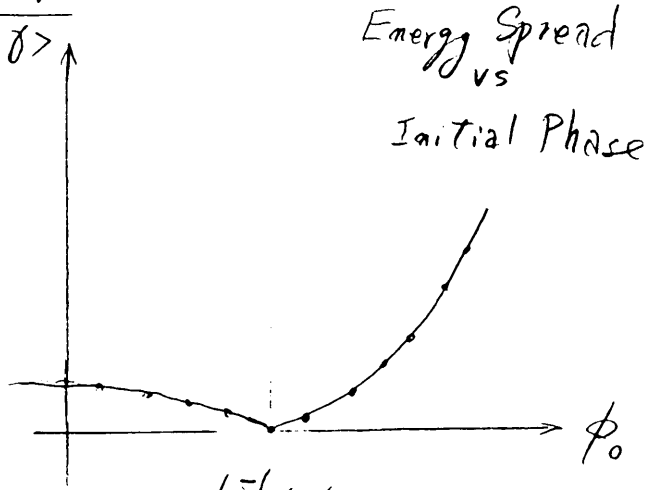

Energy Spread vs Initial Phase

$\phi^{-1}(\phi_{\gamma.pk})$

$= \phi^{-1}(78^\circ)$

Fig. 3.7

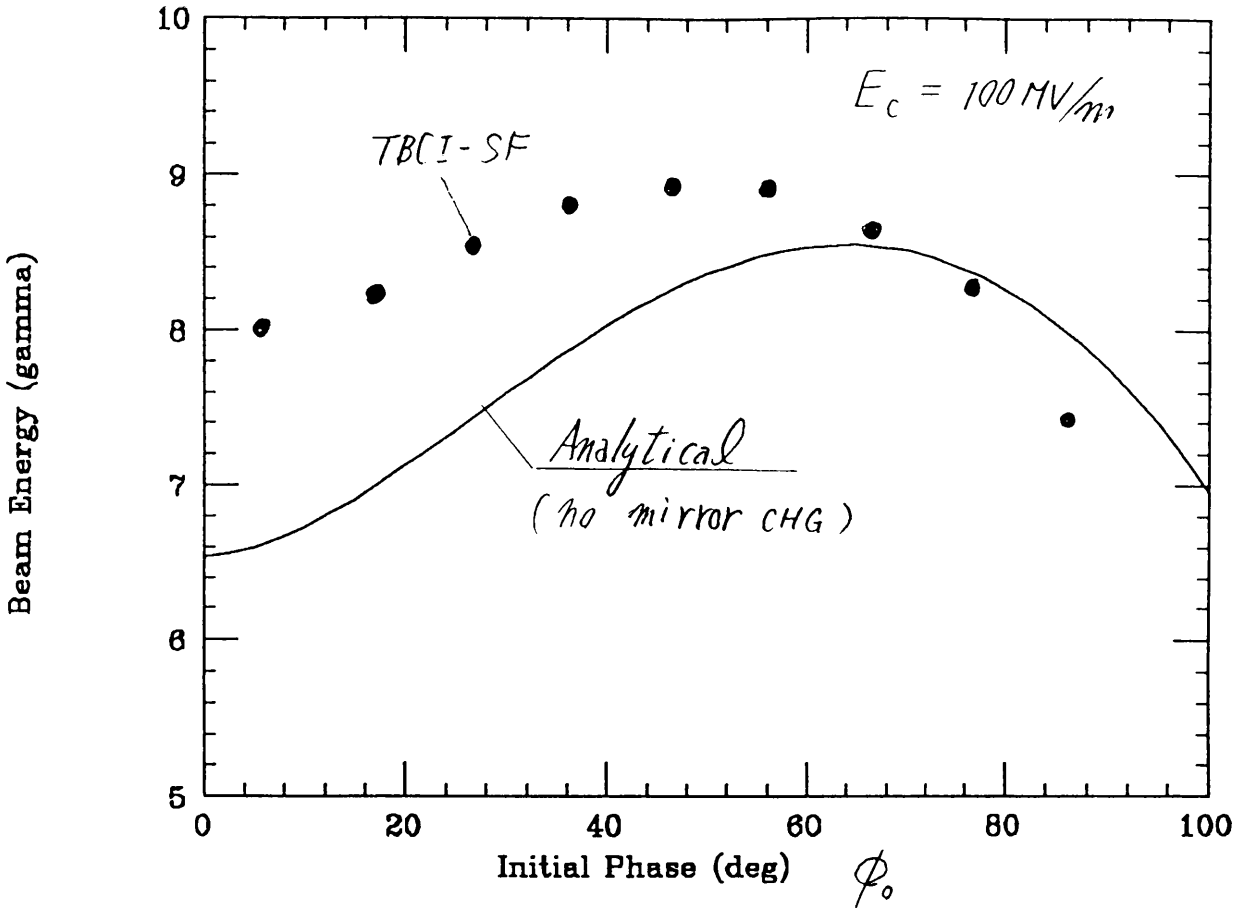
<γ>
10
9
8
7
6
5
0
20
40
60
80
100
Beam Energy (gamma)
Initial Phase (deg)
ϕ_0
E_c = 100 MV/m
TBCI-SF
Analytical
(no mirror CHG)

Fig. 3.8

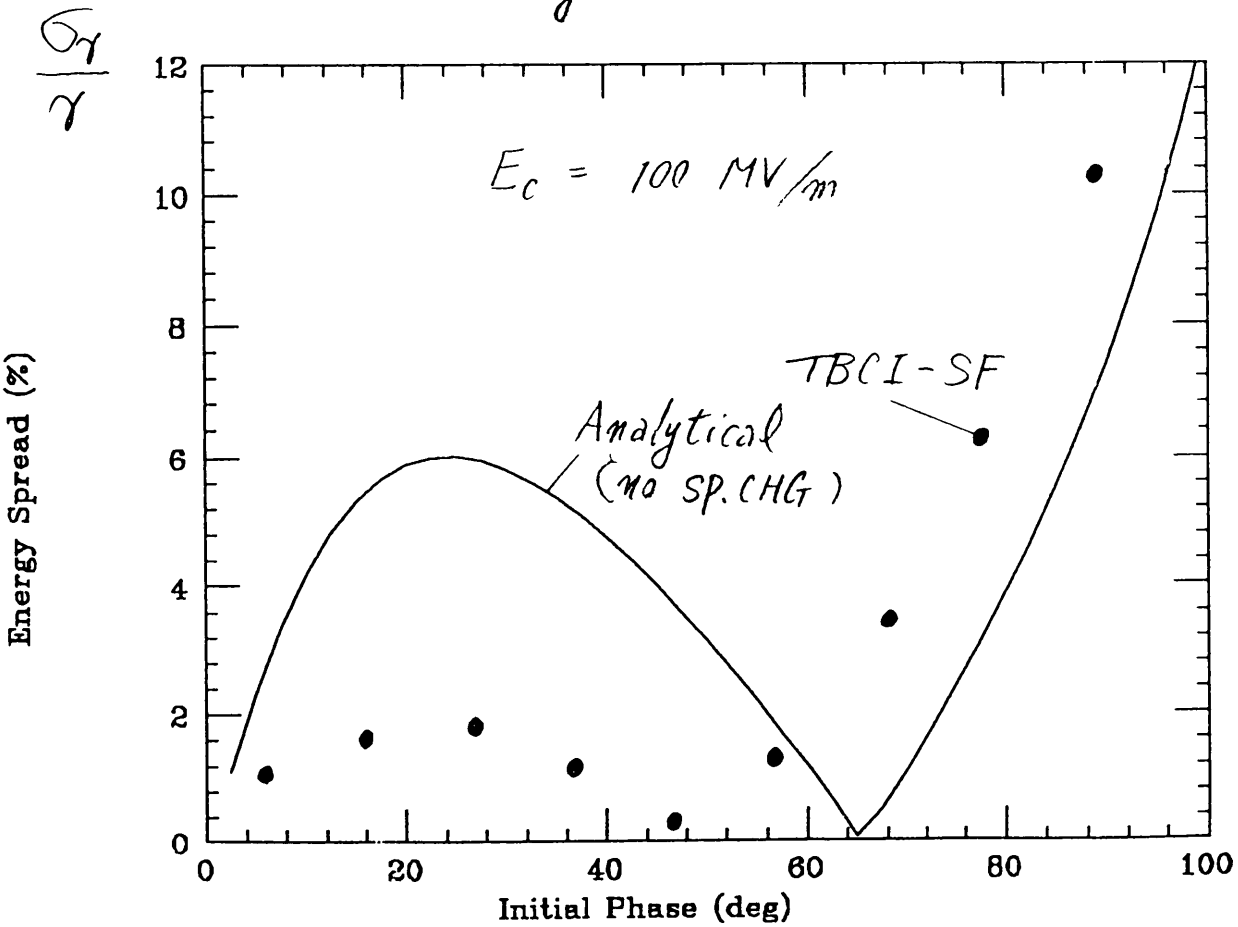
$\frac{\sigma_\gamma}{\gamma}$
12
10
8
6
4
2
0
0
20
40
60
80
100
Energy Spread (%)
Initial Phase (deg)
E_c = 100 MV/m
TBCI-SF
Analytical
(no SP. CHG)

Fig. 3.9

Fig. 4.1 Mirror Charge Effect. on the cathode

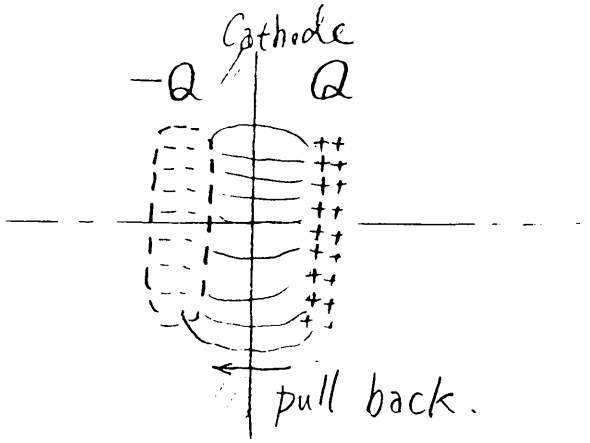

⇓ phase delay of beam start

Disk-model

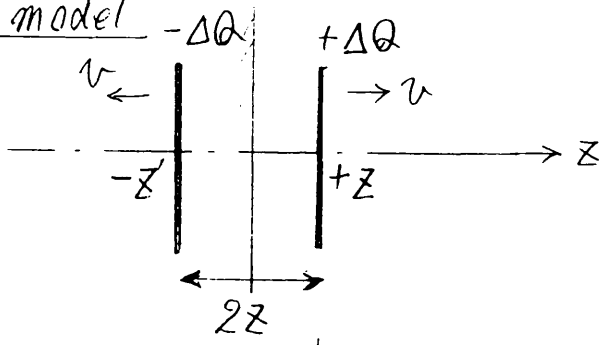

Electron rest frame

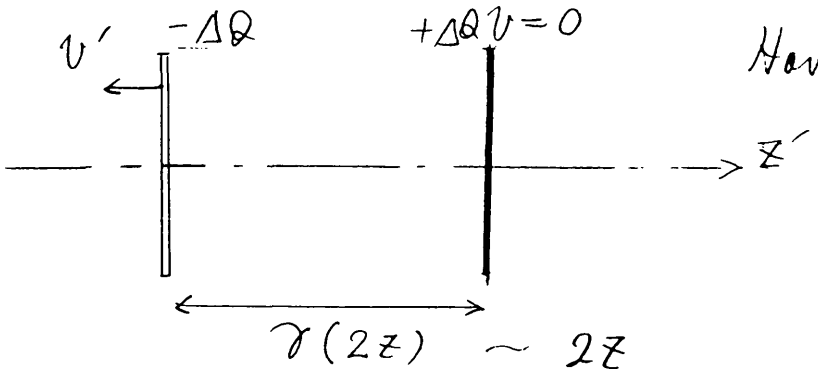

However $\gamma \sim 1$

Static Field Approximation

$$\left(\nabla^2 - \frac{\partial^2}{c^2 \partial t^2}\right)\varphi = -\frac{\rho}{\varepsilon_0}$$

⇓

$$\boxed{\nabla^2 \varphi \sim -\frac{\rho}{\varepsilon_0}}$$

Because, near cathode, $\beta \ll 1$.

F.4.1

Fig. 4.1

Small z
(plane charge field)

large z
(point charge field)

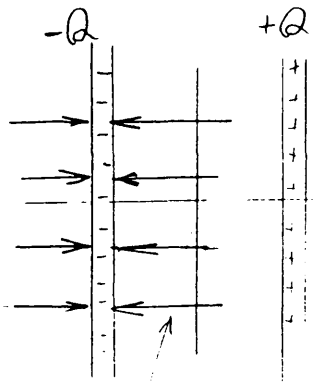

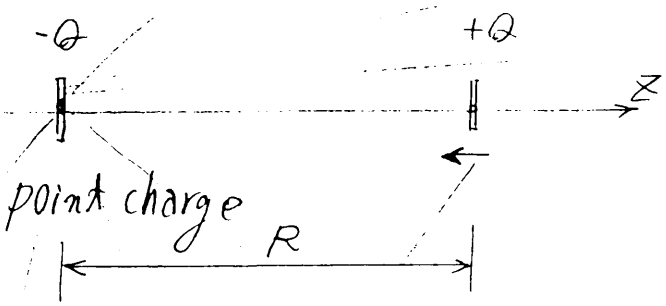

Field due to mirror charge

$$E^{0}_{z.MIR} = \frac{1}{2}\cdot\frac{\sigma_0}{\varepsilon_0} = \frac{-Q}{2\pi\varepsilon_0 r_c^2}\,, \qquad E_{z.MIR} = \frac{-Q}{4\pi\varepsilon_0 R^2}$$

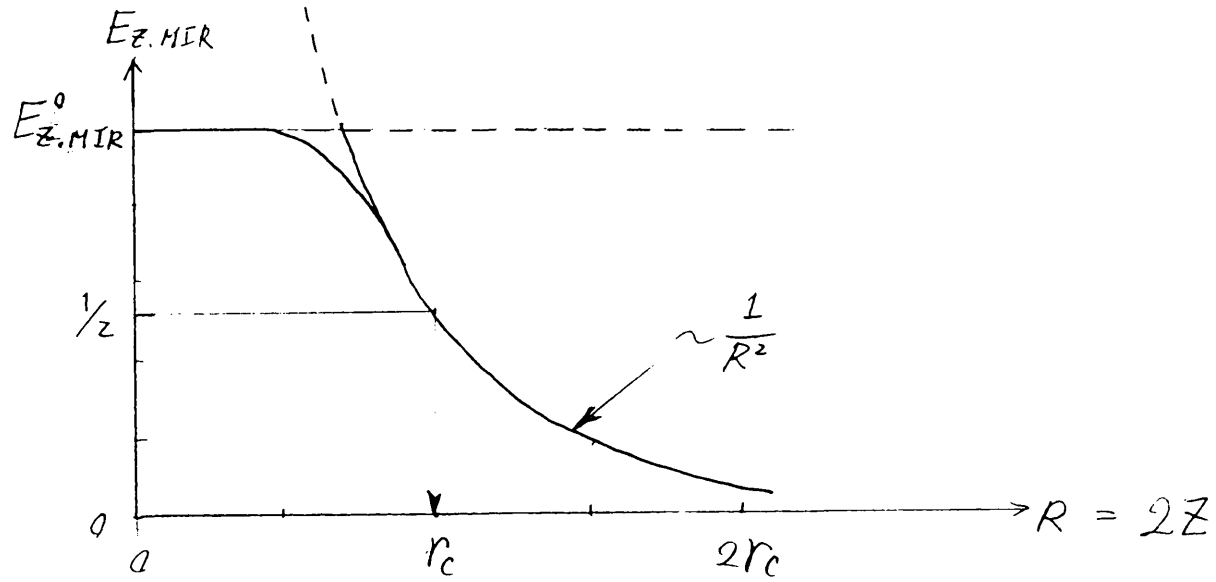

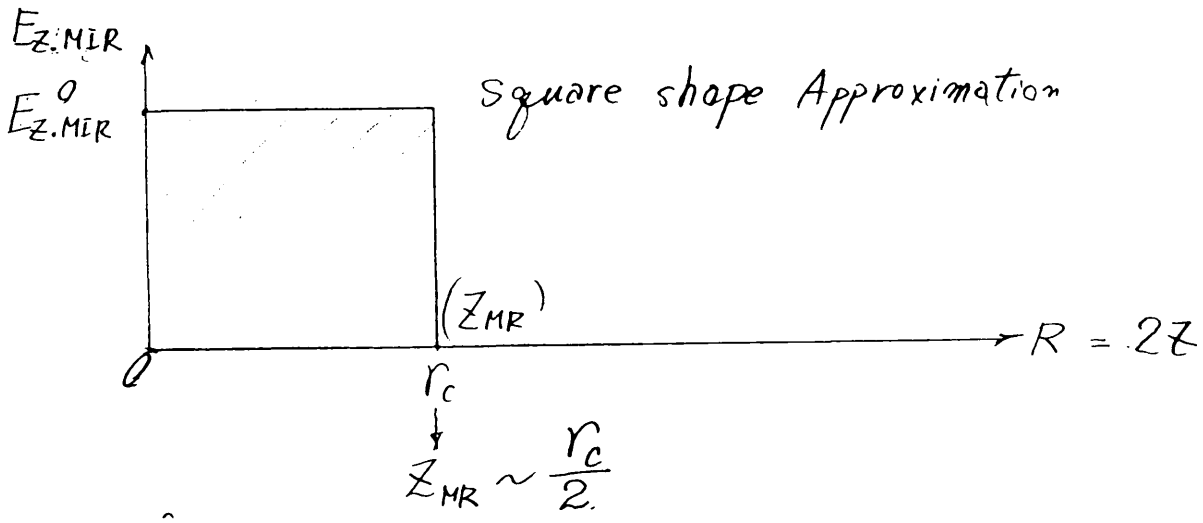

Fig. 4.2

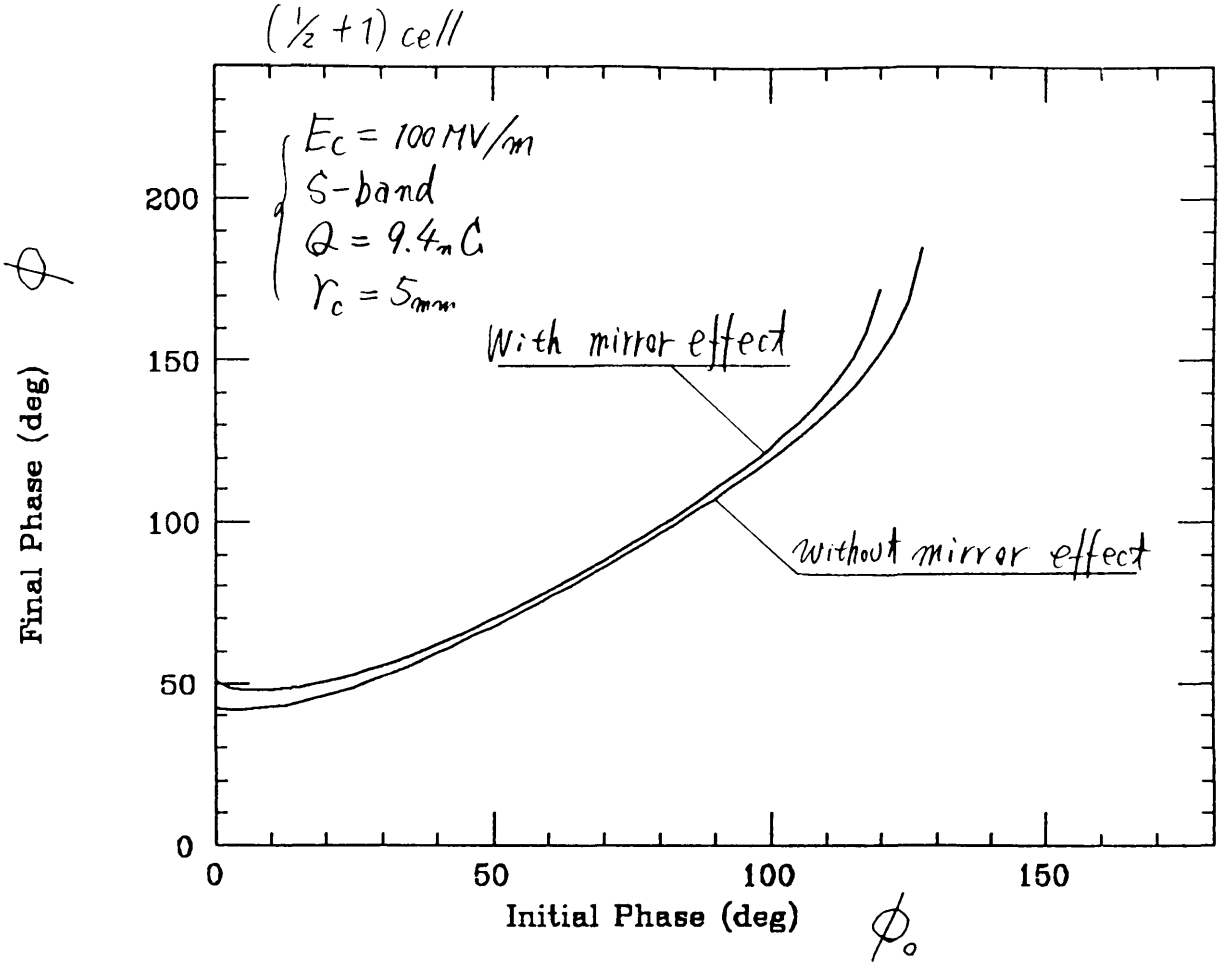

Fig. 4.3

4.3

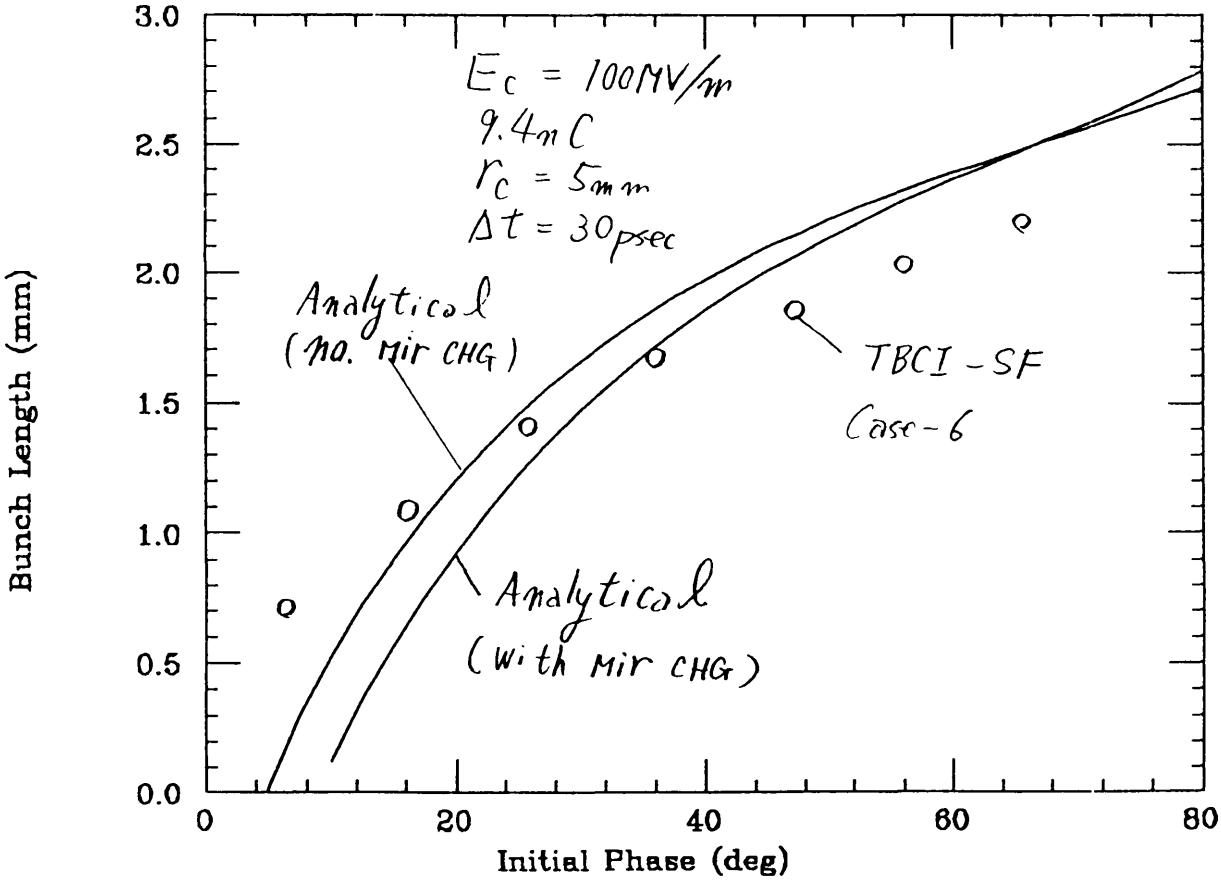

Fig. 4.4

4.4

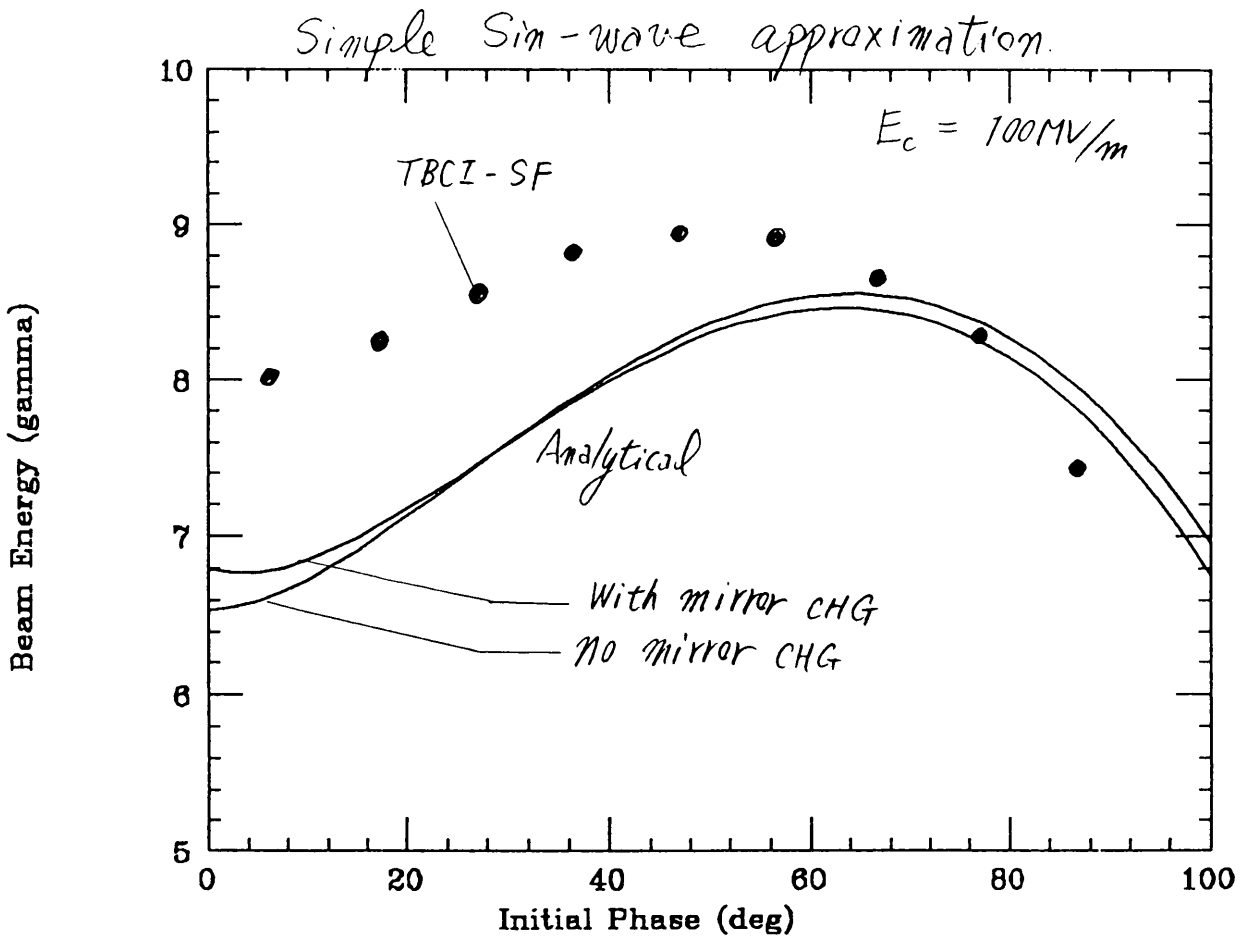
Simple Sin-wave approximation
E_c = 100MV/m
TBCI-SF
Analytical
With mirror CHG
no mirror CHG
Beam Energy (gamma)
Initial Phase (deg)
10
9
8
7
6
5
0
20
40
60
80
100

Fig. 4.5

k, 5

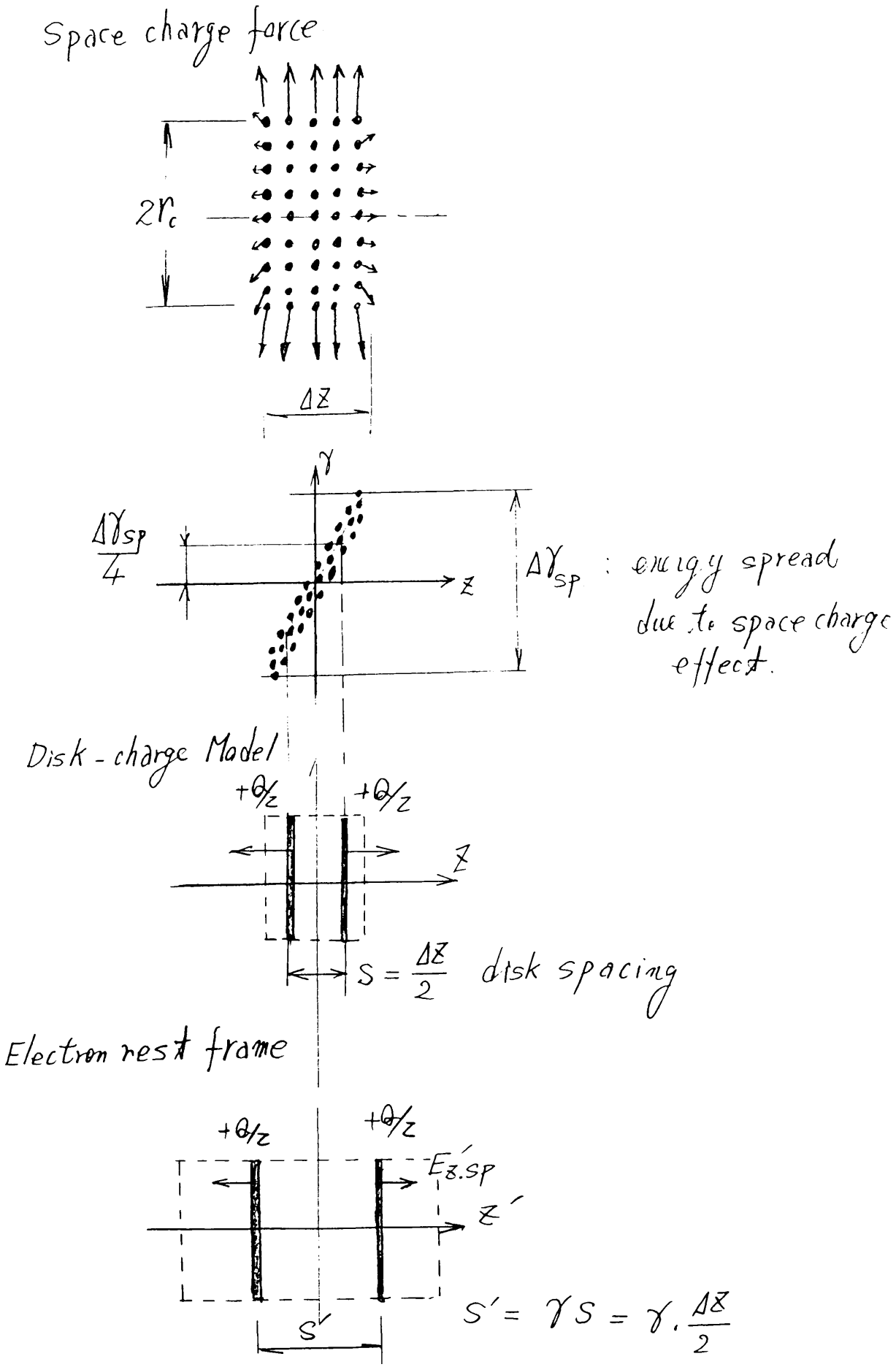
Space charge force
$2r_c$
Δz
γ
$\frac{\Delta\gamma_{sp}}{4}$
z
$\Delta\gamma_{sp}$: energy spread due to space charge effect.
Disk - charge Model
$+Q/2$
$+Q/2$
z
$S = \frac{\Delta z}{2}$ disk spacing
Electron rest frame
$+Q/2$
$+Q/2$
$E_{z.sp}'$
z'
S'
$S' = \gamma S = \gamma . \frac{\Delta z}{2}$

Fig. 5.1

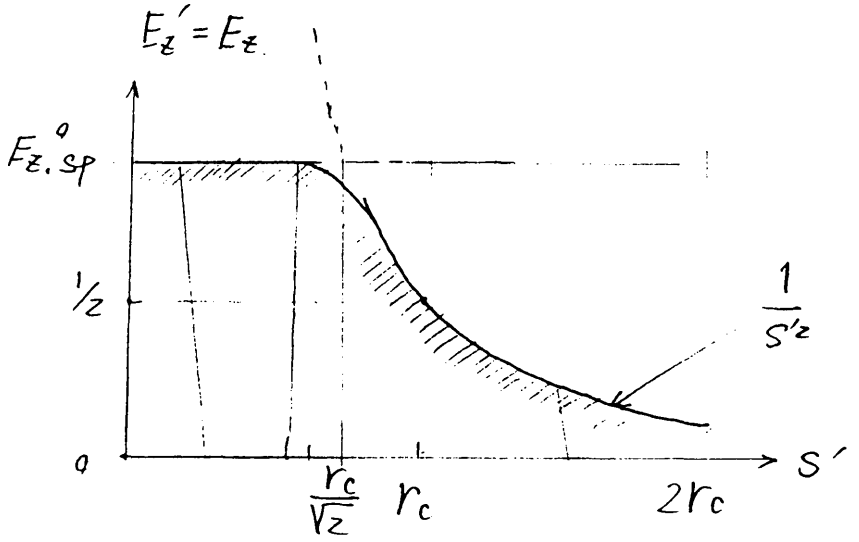

$$E_{t.sp}^{o} = \frac{+Q}{4\pi\varepsilon_0 r_c^2}$$

$$E_{t.sp} = \frac{+Q}{8\pi\varepsilon_0 s'^2}$$

Fig. 5.2

Energy Spread Cancelation

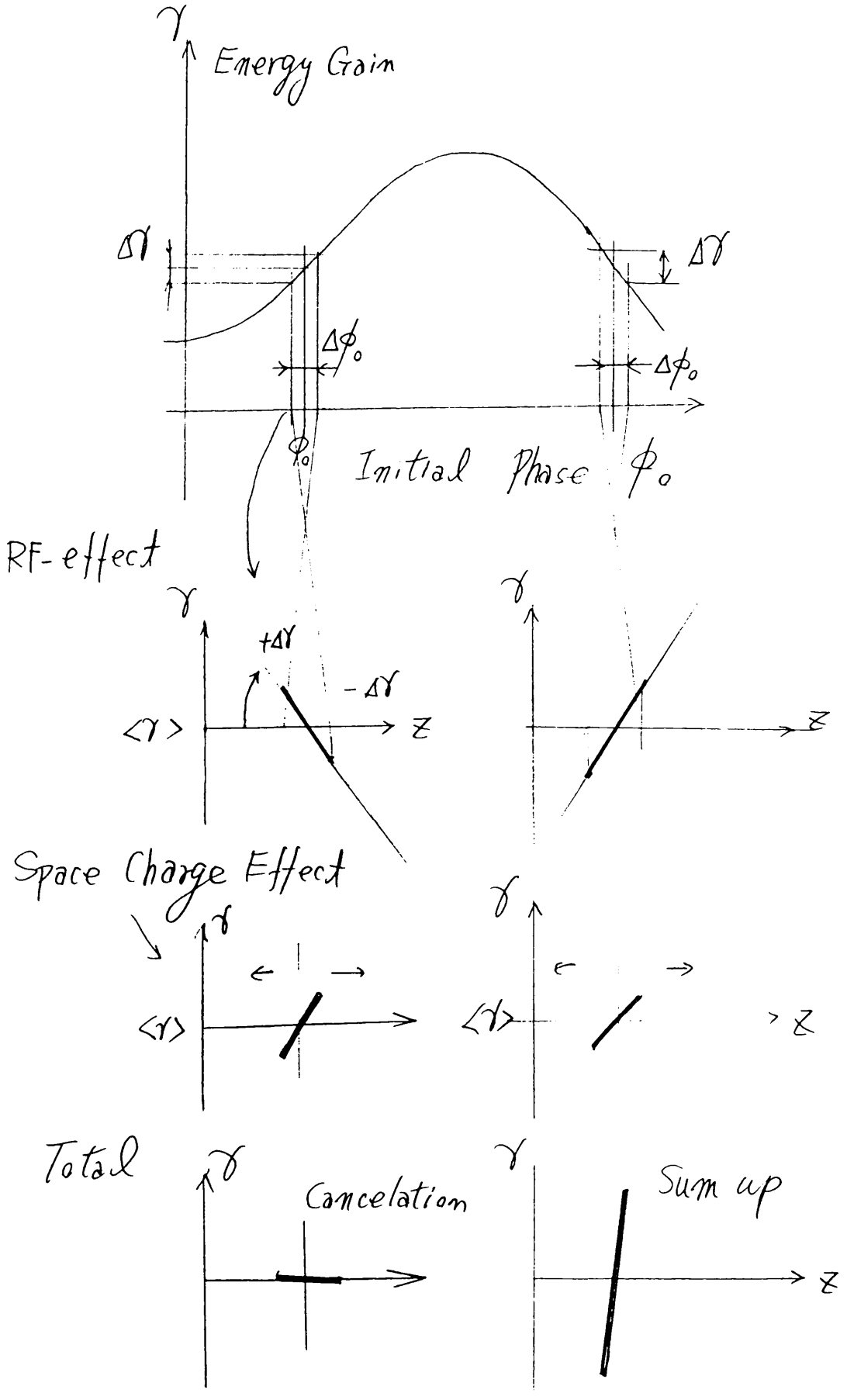

5.3

Fig. 5.3

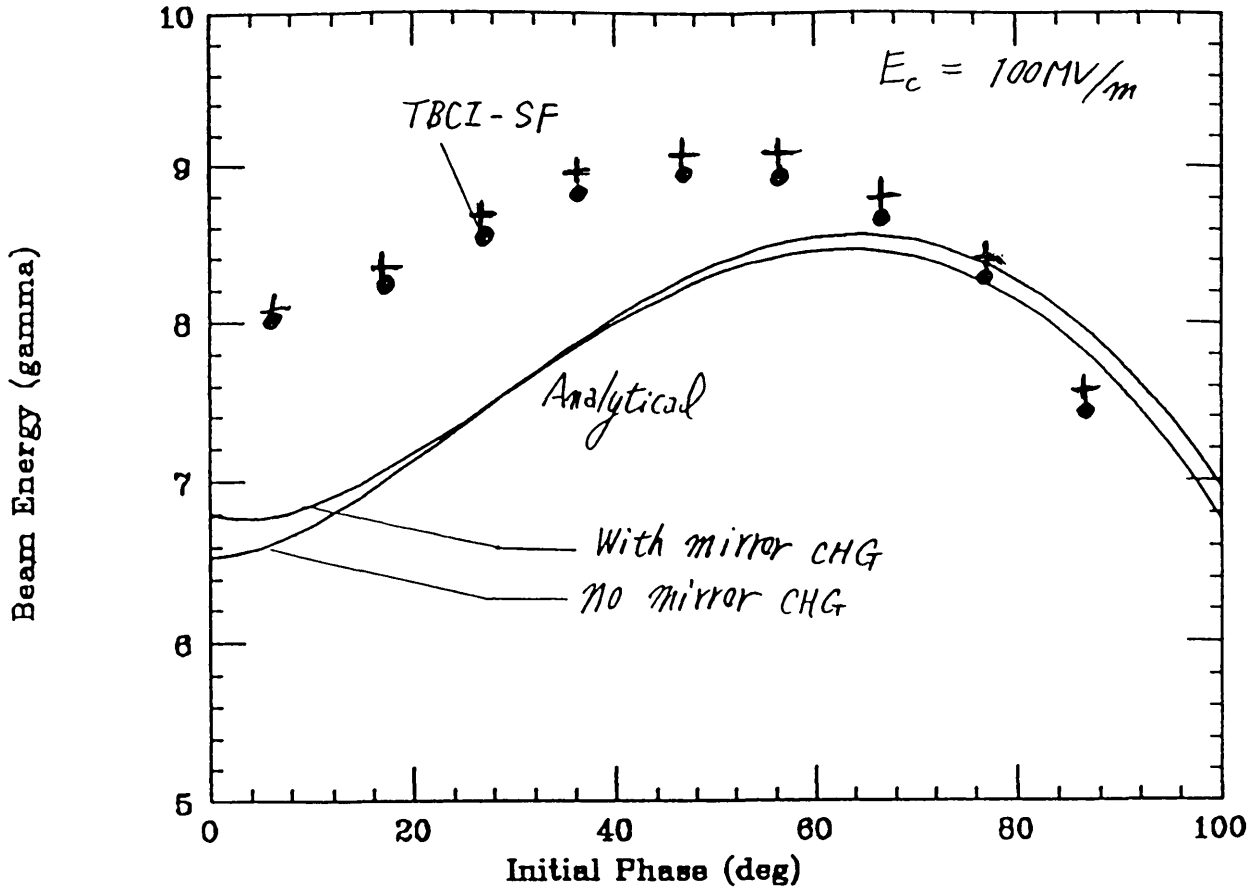

Fig. 5.4 (a)

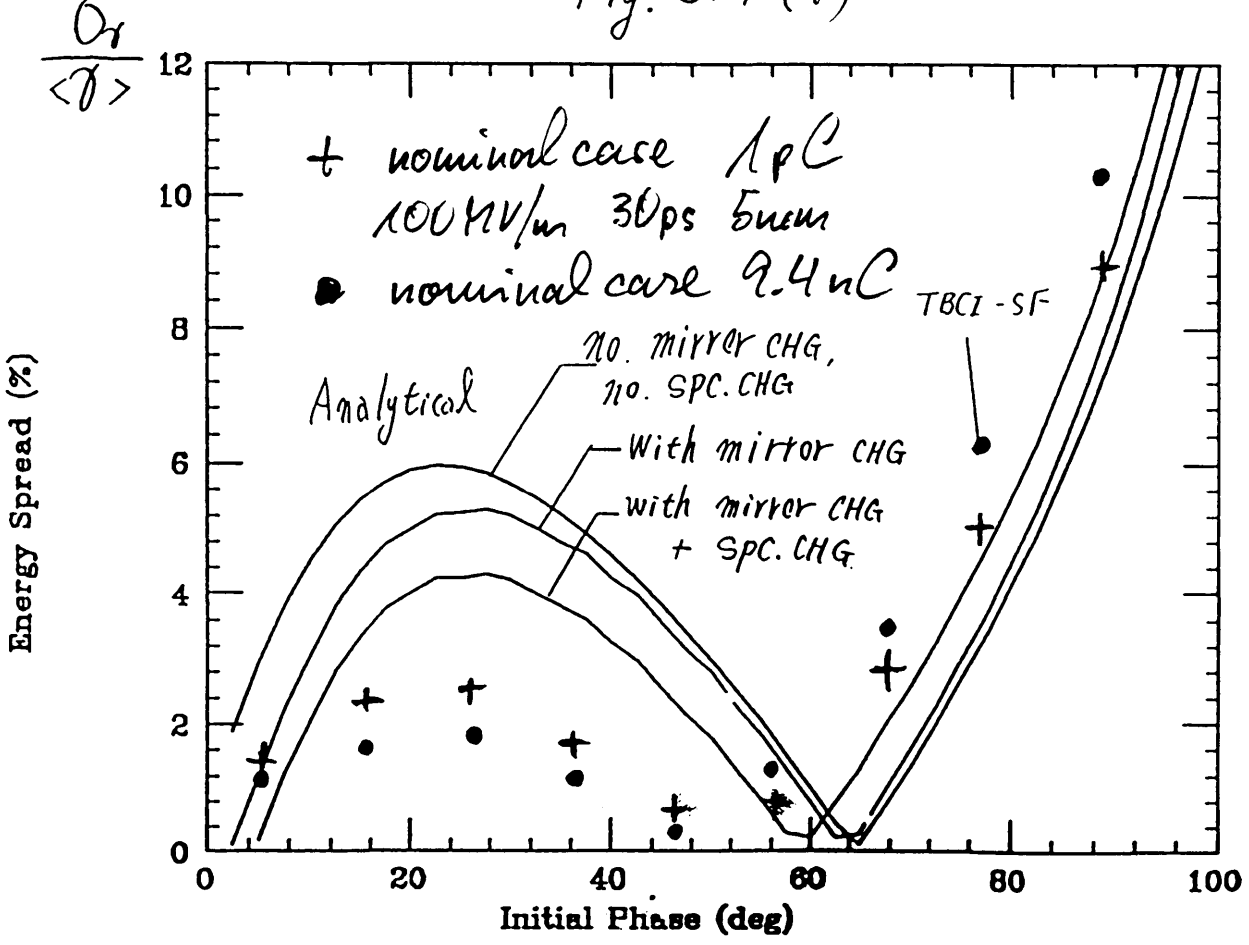

Fig. 5.4 (b)

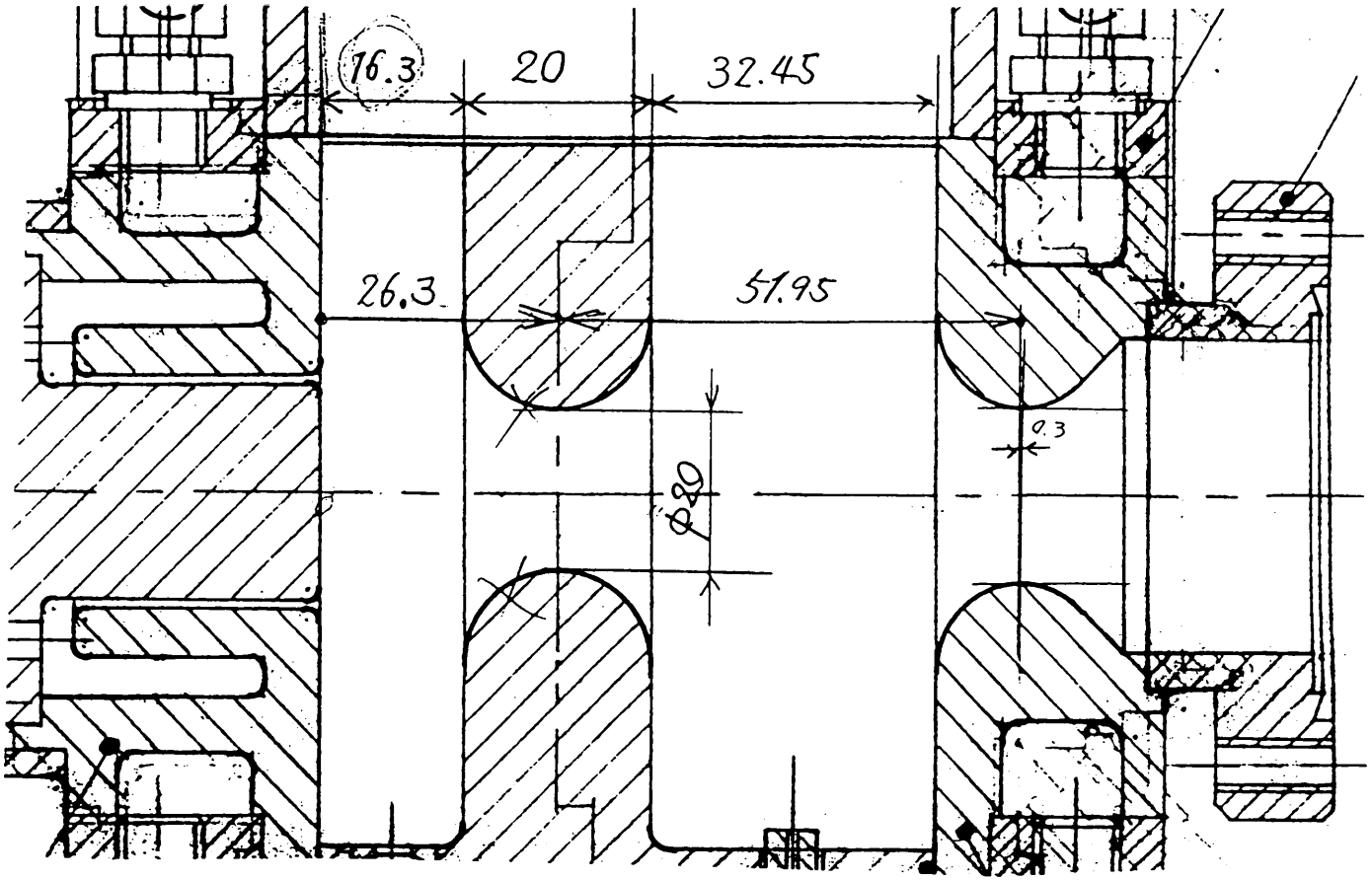
16.3
20
32.45
26.3
51.95
φ20
0.3

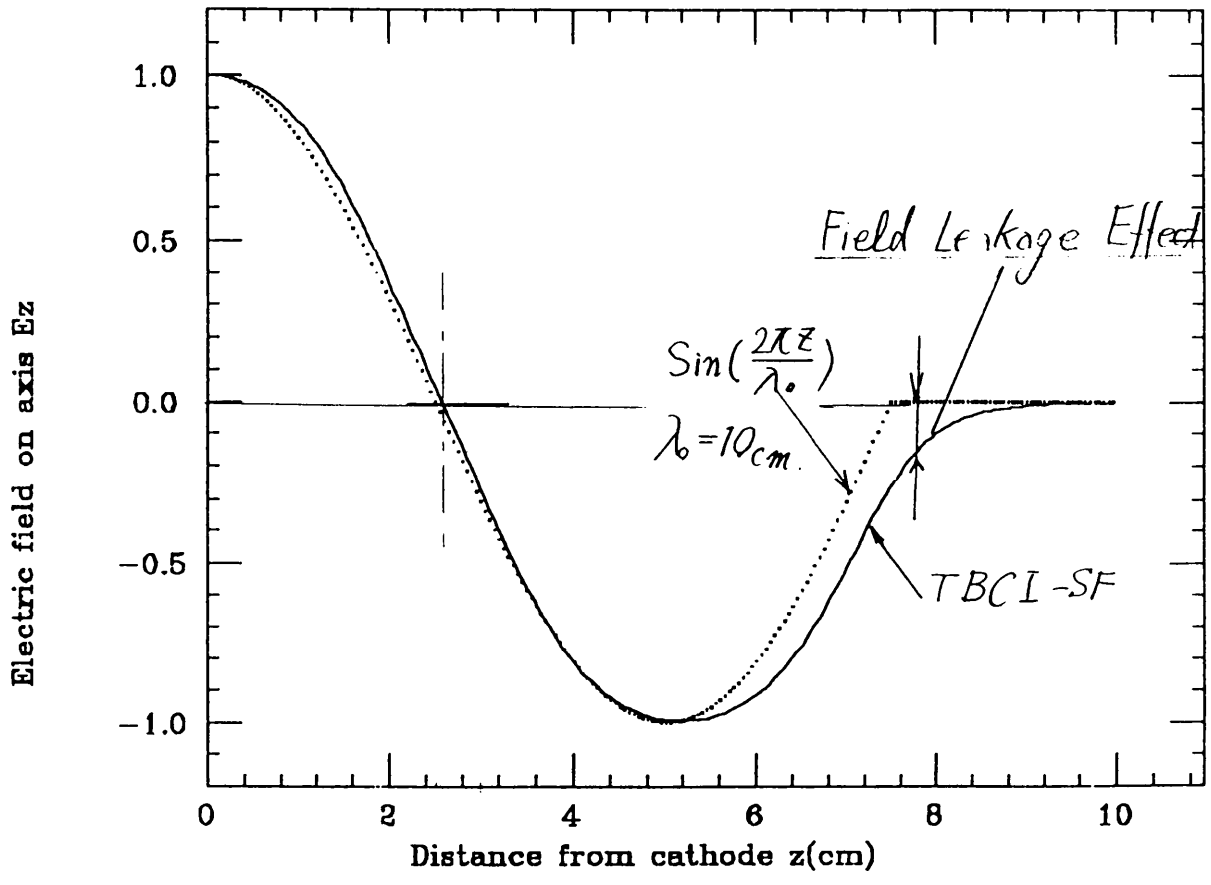
1.0
0.5
0.0
−0.5
−1.0
0
2
4
6
8
10
Electric field on axis Ez
Distance from cathode z(cm)
Field Leakage Effect
Sin(2πz/λ0)
λ0=10cm
TBCI-SF

Fig. 6.1

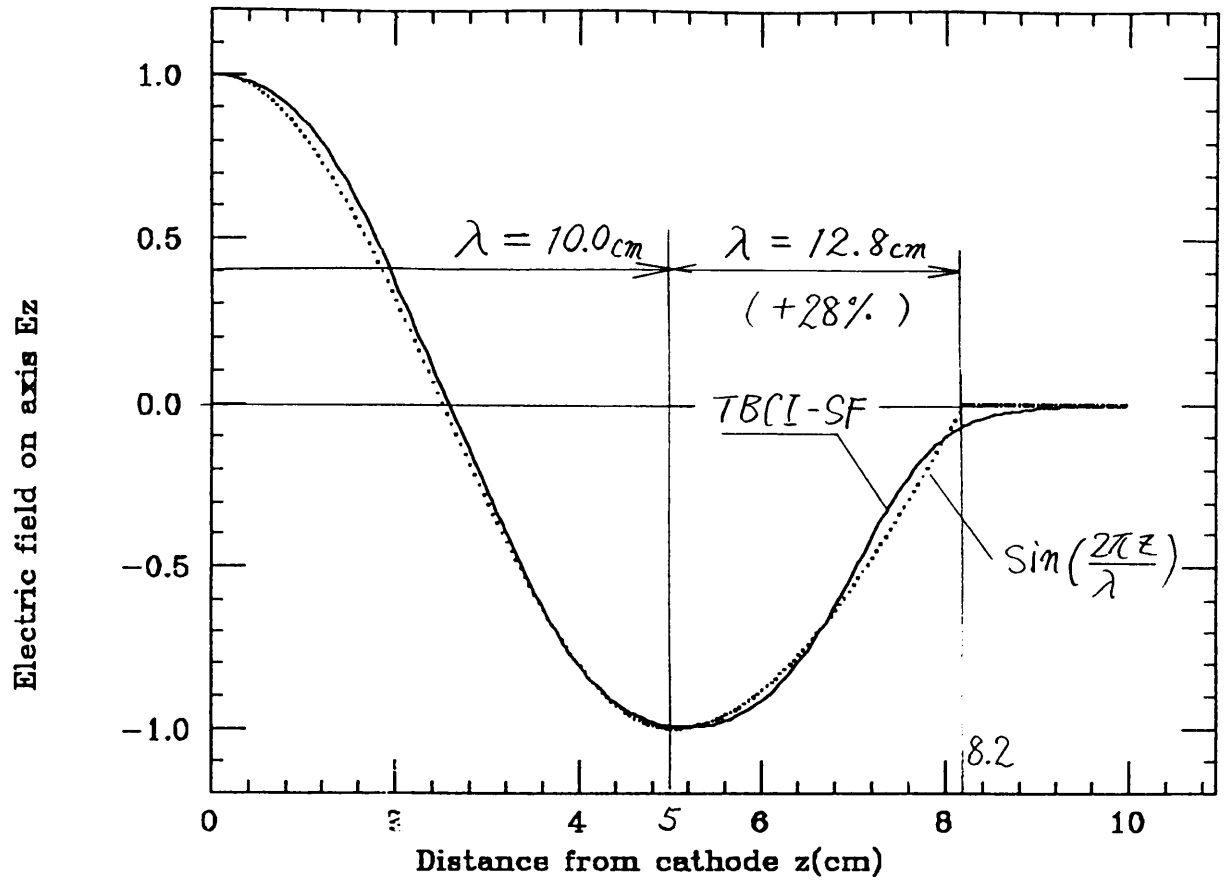

Fig. 6.2 (a)

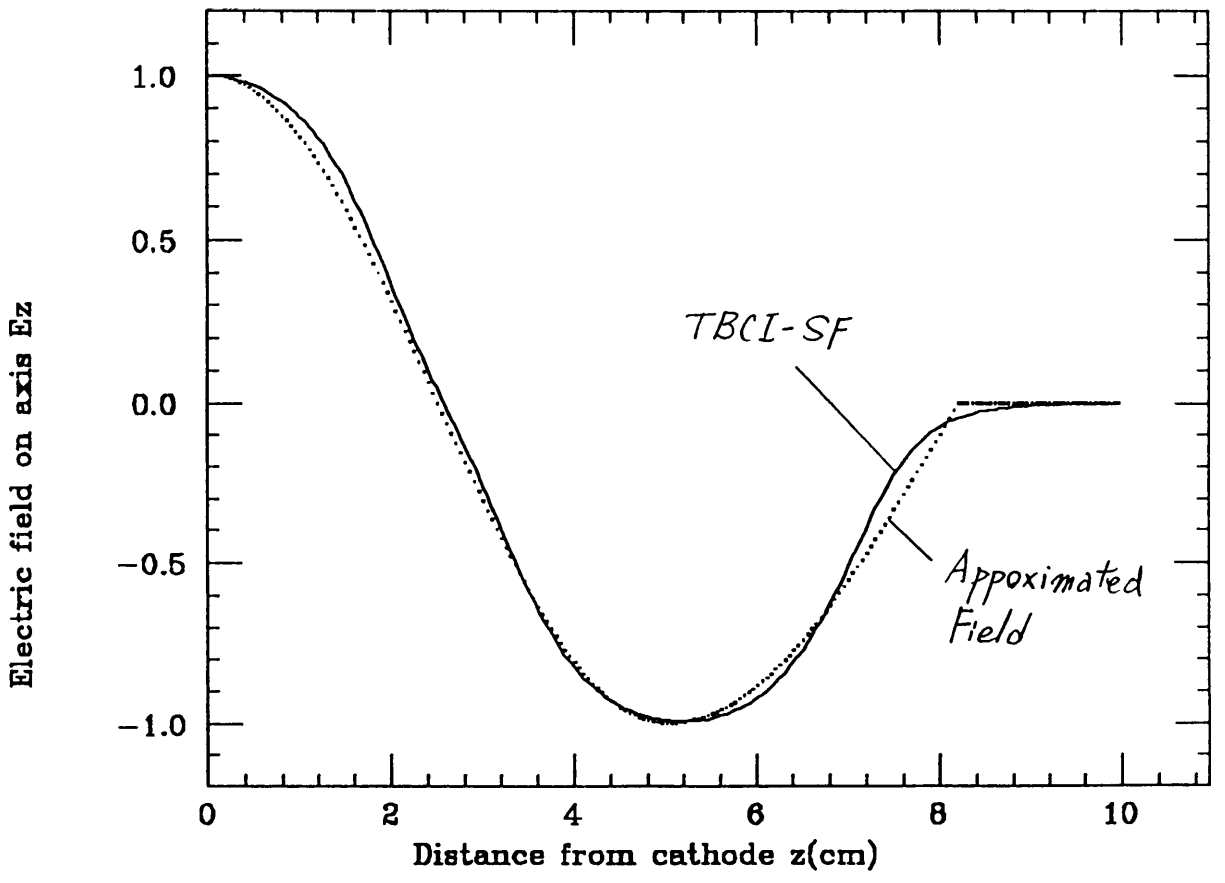

Fig. 6.2 (b)

6.2 (b)

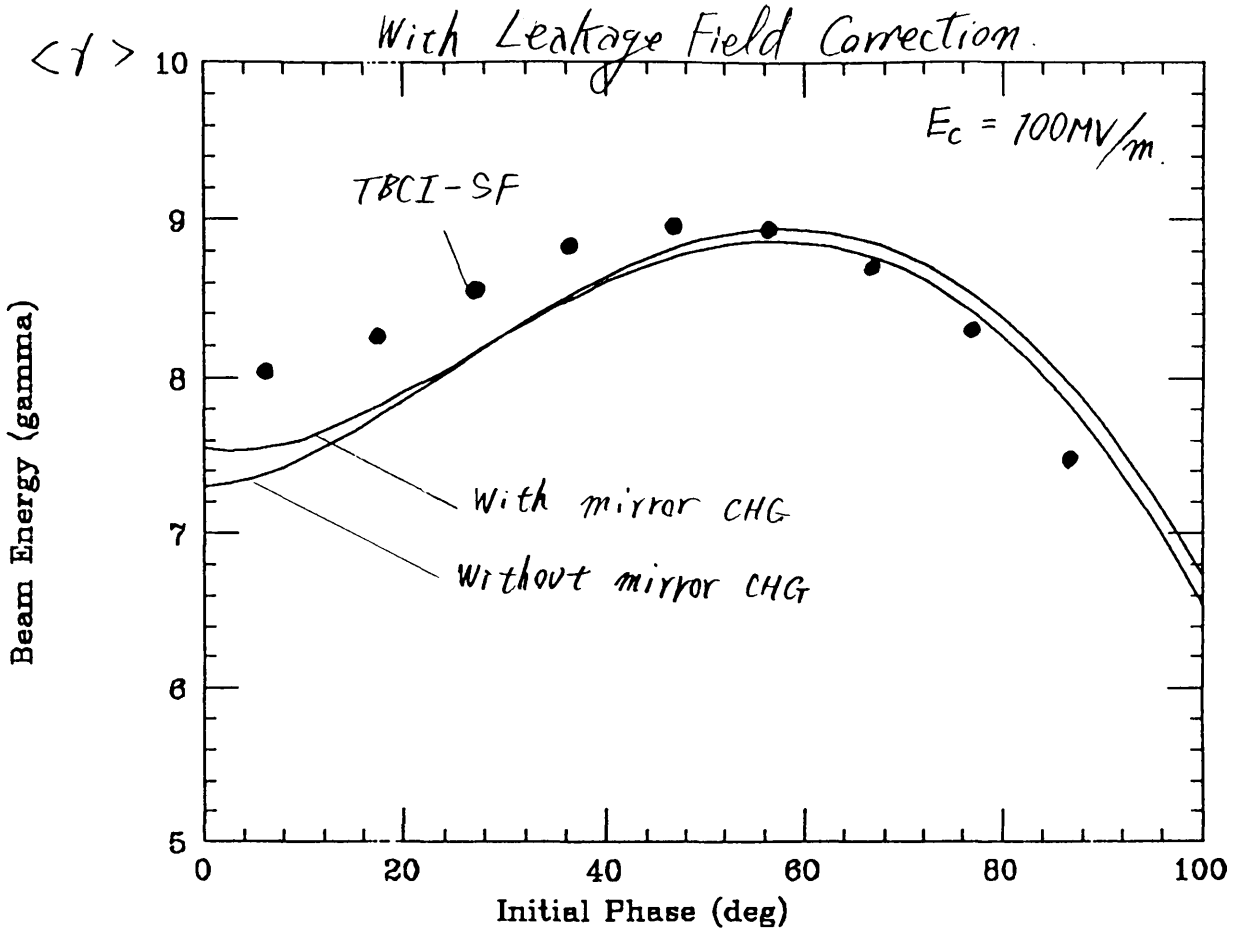

Fig. 6.3 (a)

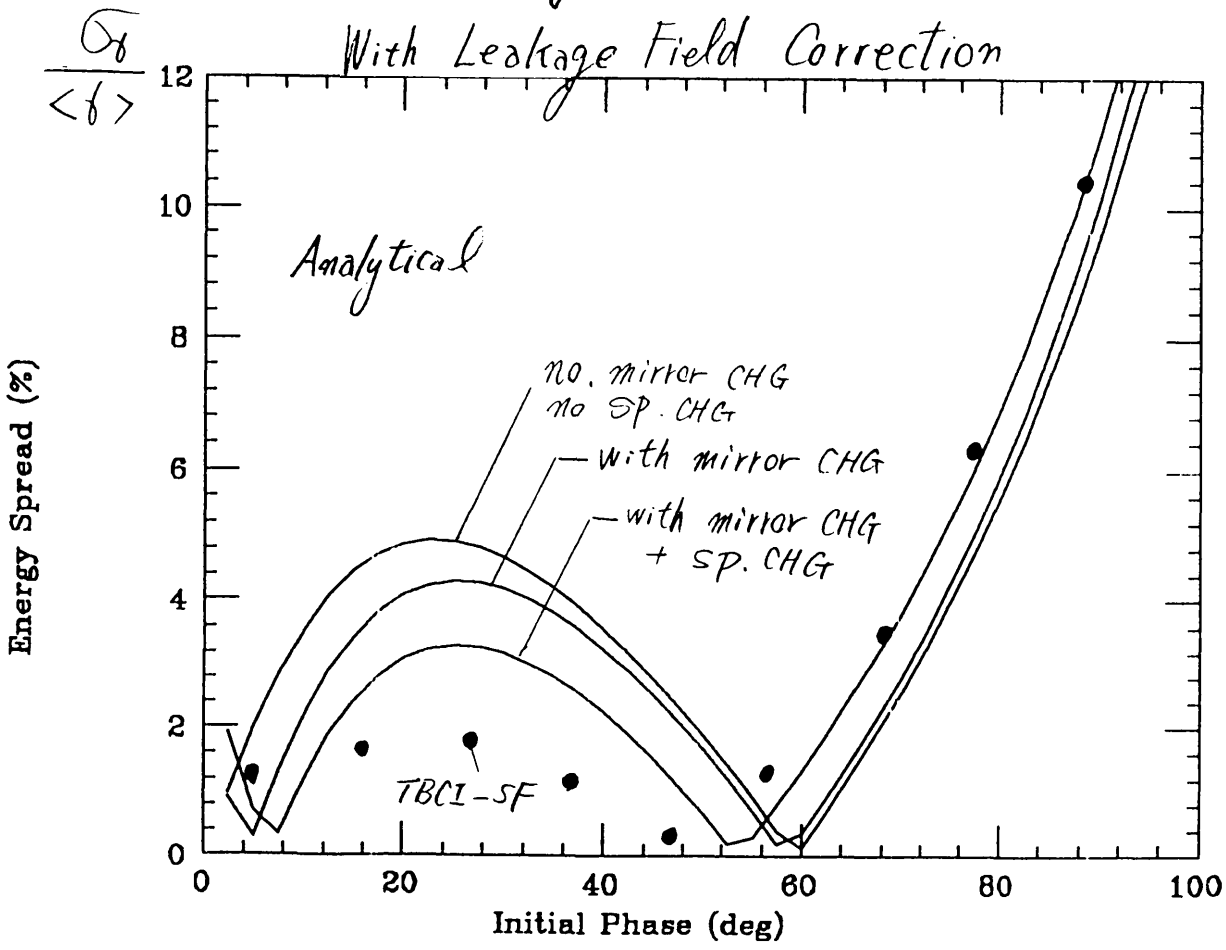

Fig. 6.3 (b)